

# Nearly-uniform internal rotation of solar-like main-sequence stars revealed by space-based asteroseismology and spectroscopic measurements

O. BENOMAR<sup>1\*</sup>, M. TAKATA<sup>1</sup>, H. SHIBAHASHI<sup>1</sup>, T. CEILLIER<sup>2</sup>, R. A. GARCÍA<sup>2</sup>

<sup>1</sup>*Department of Astronomy, School of Science, The University of Tokyo, Bunkyo-ku, Tokyo 113-0033, Japan*

<sup>2</sup>*Laboratoire AIM, CEA/DSM - CNRS - Univ. Paris Diderot - IRFU/SaP, Centre de Saclay, 91191, Gif-sur-Yvette Cedex, France*

Accepted 2015 3 July. Received 2015 May 22; in original form 2015 February 2015

## ABSTRACT

The rotation rates in the deep interior and at the surface of 22 main-sequence stars with masses between 1.0 and 1.6  $M_{\odot}$  are constrained by combining asteroseismological analysis with spectroscopic measurements. The asteroseismic data of each star are taken by the *Kepler* or CoRoT space mission. It is found that the difference between the surface rotation rate and the average rotation rate (excluding the convective core) of most of stars is small enough to suggest that an efficient process of angular momentum transport operates during and/or before the main-sequence stage of stars. If each of the surface convective zone and the underlying radiative zone, for individual stars, is assumed to rotate uniformly, the difference in the rotation rate between the two zones turns out to be no more than a factor of two in most of the stars independently of their ages.

**Key words:** asteroseismology, methods: data analysis, stars: interiors, stars: oscillations, stars: rotation, stars: solar-type

## 1 INTRODUCTION AND SUMMARY

Rotation is one of the fundamental issues that affect stellar structure and evolution. It induces material mixing processes which may have a significant influence on nucleosynthesis in stars and affects their evolution tracks. In addition, the stellar rotation plays a crucial role in the dynamo process, which is essential for the generation and maintenance of the magnetic field in stars.

A key process to understand the stellar rotation is angular momentum transport. In almost all phases of evolution, the core of stars gradually contracts, while the envelope expands, so that the rotation rate of the core is larger than that of the envelope, as long as the angular momentum is locally conserved. This general trend is compensated by the transport of the angular momentum from the core to the envelope. While many uncertainties still remain in the theoretical treatment, some clear evidences to support the presence of efficient angular momentum transport have been found in observations. Helioseismology has demonstrated nearly-uniform rotation of the Sun in the radial direction from 30 per cent of the total radius (at least) to the surface (e.g. Schou et al. 1998; Thompson et al. 2003; Eff-Darwich & Korzenik 2013). The surface rotation rates of white dwarfs, which are essentially cores of red giants, are much smaller than the value obtained by shrinking the Sun to the typical size of those stars assuming local conser-

vation of angular momentum. Asteroseismology has also recently shown that the core-to-envelope ratio of the rotation rate of several subgiants and young red giants is about 60 at most (Beck et al. 2012; Deheuvels et al. 2012, 2014), and that almost uniform rotation is detected in a main-sequence A star (Kurtz et al. 2014) and in a main-sequence F star (Saio et al. 2015). All of these results indicate that the angular momentum in the core is efficiently transported to the envelope. On the other hand, we remark that some model-dependent studies about B stars based on ground-based observation have presented only weak arguments of non-rigid rotation (Aerts et al. 2003; Pamyatnykh, Handler & Dziembowski 2004).

In spite of these results, the number of main-sequence stars in which the structure of the internal rotation has been measured is still very limited. In this paper, we present the first statistical study of the radial rotation structure for main-sequence solar-like stars. A method is proposed to constrain the ratio between the internal and surface rotation rates of a star that shows solar-like oscillations. On one hand, we measure the average interior rotation rate,  $f_{\text{seis}}$ , by asteroseismology. On the other hand, the surface rotation rate,  $f_{\text{surf}}$ , is determined either by spectroscopy or by measuring periodic luminosity variation due to stellar spots. An agreement between  $f_{\text{seis}}$  and  $f_{\text{surf}}$  implies uniform rotation, whereas a disagreement suggests a differential rotation. The determination of the core rotation rate based on high-order and low-degree p modes has been tried in helioseismology (e.g. Elsworth et al. 1995; Lazrek et al. 1996; García et al. 2004), though these have been found to be only

\* E-mail: othman.benomar@astron.s.u-tokyo.ac.jp

weakly sensitive to the solar rotation below  $0.2R_{\odot}$  (Chaplin et al. 1999; García et al. 2008). Comparison of the core rotation rate with the surface rotation rate derived from luminosity variation due to spots has been suggested in the case of solar-like pulsators by, e.g., Aerts, Christensen-Dalsgaard & Kurtz (2010). In this paper, we consider not only spots but also spectroscopic measurements to constrain the surface rotation rate, and find that the latter is more reliable.

The method has been applied to a sample of main-sequence solar-like pulsators, 20 of which have been observed by the *Kepler* mission (Borucki et al. 2010), and two by the CoRoT spacecraft (Baglin et al. 2006a,b). These are 1.0–1.6  $M_{\odot}$  stars with the solar composition, while their evolutionary stages cover the entire main-sequence phase. None of these stars are known to be members of a close binary system. In addition, they rotate faster than the Sun by (typically) an order of magnitude.

The comparison of the surface rotation rate with the average internal rotation rate shows that the two rates are generally close to each other. For 10 stars, their difference is too small to be explained by simple evolutionary models that assume local conservation of angular momentum in the radiative layers, and constant rotation rates in the convection zones. This clearly demonstrates that angular momentum is transported from the inner layers to the outer layers (in the radiative layers and/or at the interfaces between the radiative and convective zones) of these stars. The result would generally be valid for main-sequence stars with similar masses to the Sun. Under the assumption that the surface convective zone and the internal radiative zone rotate rigidly (with different rates from each other in general), we found that 21 out of 22 stars show rotation rates in the radiative interior that are consistent with those in the convective envelope within a factor of two.

The paper is structured as follows. section 2 presents how the radial structure of the rotation profile can be measured in solar-like stars. Then section 3 describes the observational constraints and the method, followed by section 4 that shows our results. Finally, section 5 is devoted to discussion.

## 2 ASTEROSEISMIC MEASUREMENT OF INTERNAL ROTATION

### 2.1 Mode properties

Asteroseismology is a powerful method to probe physical properties of invisible stellar interiors, using pulsations detected at the surface. Recent space-borne observations made by the CoRoT and *Kepler* satellites have detected oscillations of a large number of solar-like stars with an unprecedented precision (e.g. Appourchaux et al. 2012; Mathur et al. 2012), opening the possibility of scrutinising the internal structure of the stars similar to the Sun statistically (Chaplin et al. 2014). More importantly, the rotation rates both at the surface and in the deep layers have been measured for a significant number of stars at various evolutionary stages (e.g. Benomar, Appourchaux & Baudin 2009; Barban et al. 2009; Deheuvels et al. 2012, 2014; Davies et al. 2015). The measure of the internal rotation is made possible because rotation induces a splitting of oscillation eigenfrequencies, which could be compared to the Zeeman effect observed in spectral lines in presence of a magnetic field. More precisely, for a non-rotating star, a pulsation mode is described by two integers  $n$  and  $l$ , which correspond to the number of nodes along the radius of a star (radial order of the

mode<sup>1</sup>) and the number of nodal lines on the surface (degree of the mode), respectively. There exist  $2l + 1$  modes with the same  $n$  and  $l$  that have a common eigenfrequency (degenerated solutions), but different dependence on the azimuthal angle, if the star is spherically symmetric. However, the rotation lifts the degeneracy among non-radial pulsation modes ( $l > 0$ ), revealing a discrete structure of modes identified by their azimuthal order  $m$  such as  $-l \leq m \leq +l$ , with  $|m|$  equal to the number of nodal lines on the surface that coincide with meridians. Slowly rotating stars like the Sun almost preserve their spherical symmetry,<sup>2</sup> so that each mode frequency  $\nu_{n,l,m}$  is given by

$$\nu_{n,l,m} = \nu_{n,l} + m\delta\nu_{n,l}. \quad (1)$$

Here,  $\nu_{n,l}$  is the frequency for a spherically symmetric star, while  $\delta\nu_{n,l}$  is called the *rotational splitting*, which represents a small perturbation induced by the rotation. The rotational splitting is the observable parameter that enables us to measure the rotation of the stellar interior.

### 2.2 Rotational kernels

We explain how the rotational splittings are sensitive to the internal rotation profile of the star, assuming for simplicity that the rotation rate is a function of only the distance from the centre of the star. The sensitivity depends on the properties of observed oscillation modes, which are high-order (large  $n$ ) and low-degree (small  $l$ ) p modes consisting of acoustic waves, in the case of solar-like pulsators. The constituent waves can travel from the surface to deep layers before reaching their turning point, where they are refracted back toward the surface. The sensitivity of such modes to the rotation profile within the visited layers is represented by the so-called *rotational kernels*, hereafter simply referred as *kernels*,  $K_{n,l}(r)$ . The kernel of each mode mostly depends on the eigenfunction and is related to the rotational splitting,  $\delta\nu_{n,l}$ , and to the cyclic frequency of rotation,  $f(r)$ , by

$$\begin{aligned} \delta\nu_{n,l} &= (1 - C_{n,l}) \int_0^R K_{n,l}(r) f(r) dr \\ &= (1 - C_{n,l}) f_{n,l}. \end{aligned} \quad (2)$$

Thus the splitting is proportional to the average cyclic rotation frequency  $f_{n,l}$ , across the region visited by a mode of degree  $l$  and radial order  $n$ . Here,  $C_{n,l}$  is the *Ledoux* constant (Cowling & Newing 1949; Ledoux 1951). This constant measures the effect of the Coriolis force and tends toward 0 for high-order p modes. For example,  $C_{n,l} \simeq 10^{-2}$  in the range of observed modes in the Sun. This implies that the splitting may differ from the rotation frequency  $f_{n,l}$  by about 1 per cent at most. Because the typical uncertainty in the rotational splittings of solar-like stars is as large as 5 per cent, the Coriolis term  $C_{n,l}$  is in practice negligible in equation (2).

Figs 1(a) and 2(a) show examples of kernels for  $n = 10$  and  $n = 25$  for the models of the three different stars; the Sun (Christensen-Dalsgaard et al. 1996), *Kepler-25* ( $M = 1.26 \pm 0.03 M_{\odot}$ , see Benomar et al. 2014b) and HAT-P-7 ( $M = 1.59 \pm$

<sup>1</sup> This is only an approximate explanation about the radial order. More detailed discussion is found in Takata (2012).

<sup>2</sup> Strictly speaking, the effect of the centrifugal force that causes distortion of the stellar configuration might not always be negligible in the stars dealt in this paper, because they rotate significantly faster than the Sun. This problem is discussed in section 3.3. On the other hand, we assume for simplicity that the effect of the magnetic field is much smaller than that of rotation.

0.03  $M_{\odot}$ , Benomar et al. 2014b; Lund et al. 2014). Only modes of degrees  $l = 1$  and  $l = 2$  are shown, as it is rare to observe  $l = 3$  (and higher-degree) modes in *Kepler* or CoRoT data. The radius is normalised by the stellar radius  $R$  in each case. The kernels are denser and of greater amplitude near the stellar surface, indicating that the sensitivity to the rotation is the highest close to the surface. This reflects the fact that acoustic waves, the main constituents of high-order p modes, slow down as they come close to the surface, so that the mode periods, which are essentially determined by the residence time of the waves at each layer, are most influenced by the near-surface structure. Note that at the outer edge of the convective core of *Kepler 25* and HAT-P-7, a small kernel discontinuity appears. This is caused by those of the chemical composition at the top of the convective core and is due to the fact that diffusion is neglected in our models.

Figs 1(b) and 2(b) show the cumulative integrals  $\int_0^{r_0} K_{n,l}(r) dr$  for degrees  $l = 1$  and  $l = 2$ , respectively. Note that within the observable range of  $n$ , which is approximately between 10 and 25, all of the kernels with  $l = 1$  and  $l = 2$  are nearly identical to each other. Still, there is clear dependence of the base of the convective envelope on the mass, such that more massive stars have shallower convective envelopes. This implies that the contribution of the radiative zone to the rotational splittings is greater in more massive stars than in less massive ones. Furthermore, the profiles in the radiative zone are almost linear functions of radius, between  $\sim 0.15R$  and the outer edge of the zone. Since the gradient of the profiles indicates the sensitivity to each layer, each observed eigenmode probes the radiative zone nearly uniformly from the very deep inner layers to the outer edge.

### 2.3 Rotation rates in the envelope and in the radiative zone

A solar-like star (slightly more massive than the Sun) consists of an outer convective zone, an intermediate radiative zone and a core where nuclear fusion occurs. Figs 1 and 2 demonstrate that low-degree modes are insensitive to the stellar core. In order to probe the rotation rate within the (radiative) core, it is required to measure g modes (e.g. García, Mathur & Ballot 2008; Mathur et al. 2008; Appourchaux et al. 2010), which are still elusive in solar-like stars, or mixed modes (e.g. Deheuvels et al. 2014), which are seen in evolved solar-like stars only. However, we stress that the rotational splittings of low-degree p modes in main-sequence solar-like stars are sensitive to the rest of the structure, both of the radiative zone and the convective envelope.

In order to separate the contributions from the radiative and (outer) convective zones, it is assumed that the two zones rotate uniformly with different rates along the same axis. Then, it is possible to express the rotational splitting,  $\delta\nu_{n,l}$ , by a weighted average of the rotation rate of the radiative zone,  $f_{\text{rad}}$ , and that of the convective zone,  $f_{\text{conv}}$ , as

$$\delta\nu_{n,l} \simeq I_{\text{rad}} f_{\text{rad}} + I_{\text{conv}} f_{\text{conv}}, \quad (3)$$

where  $I_{\text{rad}} = \int_0^{r_c} K_{n,l}(r) dr$  and  $I_{\text{conv}} = \int_{r_c}^R K_{n,l}(r) dr$  denote the integrals of the kernel in the radiative and convective zones, respectively, with  $r_c$  being the radius at the base of the convective zone. Note that

$$I_{\text{conv}} + I_{\text{rad}} = 1, \quad (4)$$

because each kernel is normalised to 1.

It is required to make two additional assumptions in order to make use of equation (3). Firstly, the rotation rate in the convective envelope,  $f_{\text{conv}}$ , is assumed to be equal to that at the

surface,  $f_{\text{surf}}$ . This is supported by the solar case, which shows 30 per cent difference at most in the rotation rate in the latitudinal direction and much smaller in the radial direction in the convection zone (e.g. Schou et al. 1998; Thompson et al. 2003; Eff-Darwich & Korzennik 2013). Secondly, it is assumed that the rotational splittings remain nearly constant over the observed ranges of  $n$  and  $l$ , so that the average rotational splitting,  $\langle\delta\nu_{n,l}\rangle$ , can be used as a representative value of the seismically measured internal rotation rate,  $f_{\text{seis}}$ . This point has been justified in section 2.2 by demonstrating that the integrals of the kernels of the observed p modes differ little from each other. We can now use equation (3) to express the relation linking the surface rotation rate,  $f_{\text{surf}}$ , the average rotation rate in the radiative zone,  $\langle f_{\text{rad}} \rangle$ , and the average rotation rate of the stellar interior,  $f_{\text{seis}} = \langle\delta\nu_{n,l}\rangle$ , as

$$\langle f_{\text{rad}} \rangle = f_{\text{surf}} + \langle I_{\text{rad}} \rangle^{-1} (f_{\text{seis}} - f_{\text{surf}}). \quad (5)$$

Note that  $\langle \rangle$  denotes the average values over the range of observed  $n$  and  $l$ , with  $10 \lesssim n \lesssim 25$  and  $1 \leq l \leq 2$ .

If we go back to equation (3), it tells that  $f_{\text{seis}}$  is reduced to a simple average of  $f_{\text{rad}}$  and  $f_{\text{conv}}$ , if  $\langle I_{\text{rad}} \rangle = \langle I_{\text{conv}} \rangle$ . However, in stars with a thin convective envelope (*i.e.* the most massive solar-like stars), the sensitivity of the splitting to the rotation within the radiative zone may dominate, which means  $\langle I_{\text{rad}} \rangle \gg \langle I_{\text{conv}} \rangle$ , so that these stars are ideal candidates to probe a differential rate between outer and inner layers. In fact, equation (5) is equivalent to  $f_{\text{seis}} - f_{\text{surf}} = \langle I_{\text{rad}} \rangle (\langle f_{\text{rad}} \rangle - \langle f_{\text{conv}} \rangle)$ , whose left-hand side is an observable. This equation shows that, for a given difference in the rotation rate between the radiative zone and the convective envelope, the observed difference between  $f_{\text{seis}}$  and  $f_{\text{surf}}$  is larger (in magnitude) in stars with larger  $\langle I_{\text{rad}} \rangle$ .

Applying the error propagation law to equation (5), we estimate that an interior with faster-than-surface rotation can be detected at a  $1\sigma$  detection level if  $(f_{\text{seis}} - f_{\text{surf}})/f_{\text{surf}} \gtrsim 25$  per cent, which corresponds to  $\langle f_{\text{rad}} \rangle/f_{\text{surf}} \gtrsim 1.5$ . Similarly, detecting a slower-than-surface rotation requires  $(f_{\text{seis}} - f_{\text{surf}})/f_{\text{surf}} \lesssim -45$  per cent, or  $\langle f_{\text{rad}} \rangle/f_{\text{surf}} \lesssim 0.2$ . This is obtained by assuming that the relative uncertainty on  $f_{\text{surf}}$  is of 30 per cent, based on the Sun. Here, the uncertainty account for the fact that  $f_{\text{conv}}$  and  $f_{\text{surf}}$  may not be identical, depending on the latitude at which the star is observed (latitudinal differential rotation)<sup>3</sup>. We also set the uncertainties on  $f_{\text{seis}}$  to 5 per cent and to 4 per cent on  $\langle I_{\text{rad}} \rangle$  (justified in section 4).

In the following, equation (5) is used to measure the rotation rate in the radiative zone.

## 3 DERIVING THE STELLAR ROTATION

This section describes how the surface and internal rotation is derived from the observables.

### 3.1 Surface rotation rate

The surface rotation rate  $f_{\text{surf}}$  can be estimated using either (1) rotational broadening of spectroscopic absorption lines, which gives  $v \sin i = 2\pi R f_{\text{surf}}^{(1)} \sin i$ , with the radius,  $R$ , and the inclination angle,  $i$ , determined by theoretical models and asteroseismic analysis, respectively, or (2) the brightness modulation of period

<sup>3</sup> Actually, this is a very conservative value as our formal uncertainties on  $f_{\text{surf}}$  are in fact of  $\approx 10$  per cent.

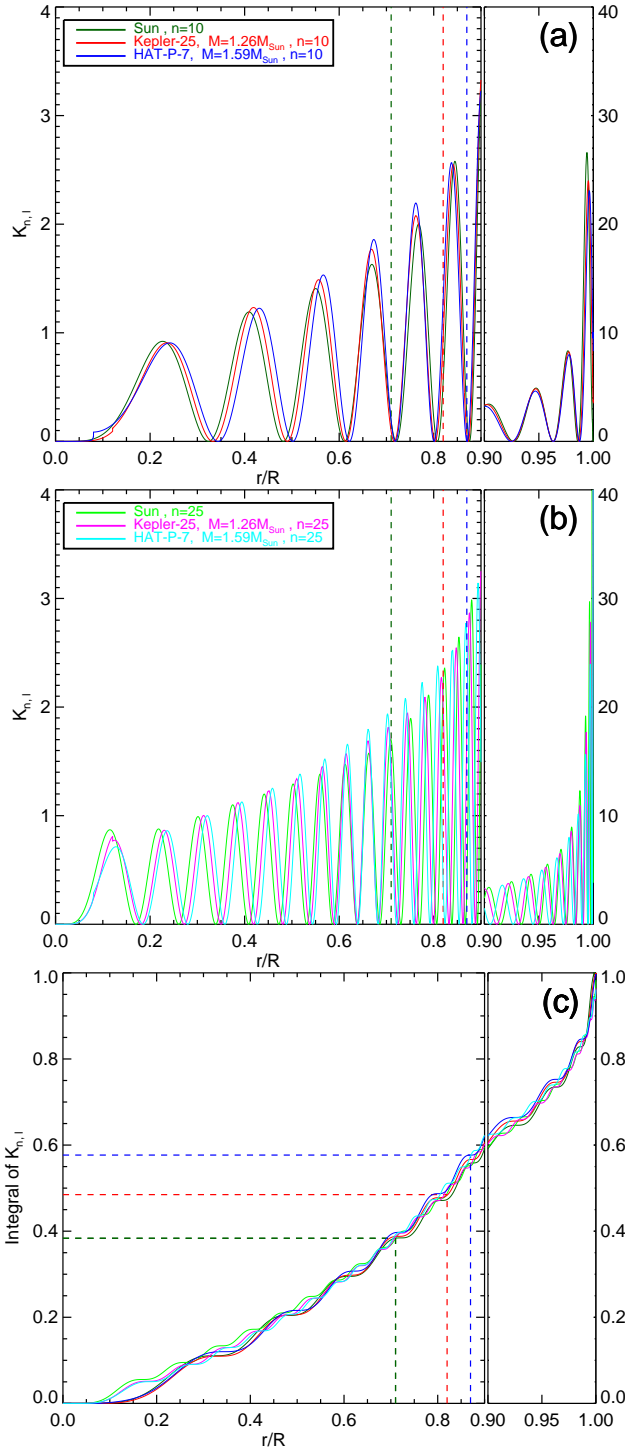


**Figure 1.** The figures show the rotational kernels (a,b) and their integral over the radius (c) for the Sun, *Kepler-25* and *HAT-P-7* for  $l = 1$  modes. Plots have two scales to magnify the Kernel of near-surface layers. Only modes with radial orders  $n = 10$  (a) and  $n = 25$  (b) are shown. Integrals of kernels are almost identical to each other independently of the star. Vertical dotted lines indicate bases of the outer convective zones. Small discontinuities around 0.1 in (a) and (b) are caused by those of the chemical composition at the top of the convective core.

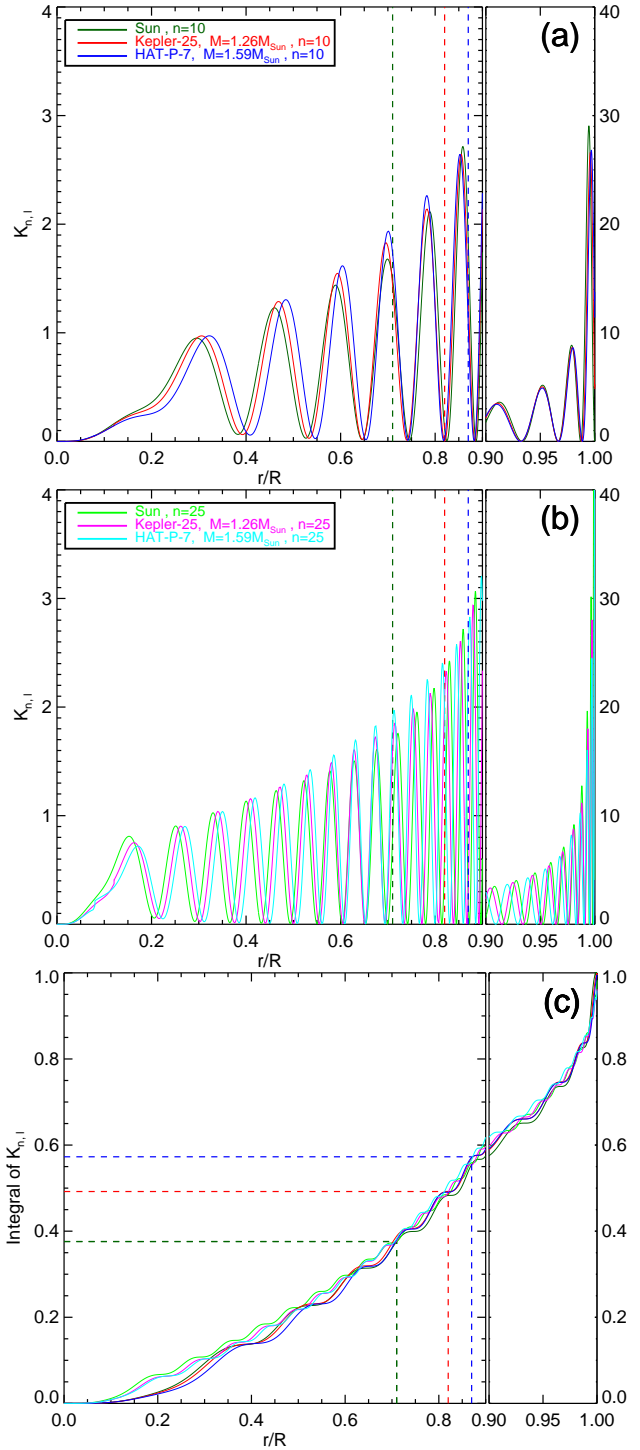


**Figure 2.** Same as Fig. 1, but for  $l = 2$  modes.

$P_{\text{rot}} = 1/f_{\text{surf}}^{(2)}$  due to structures at the surface of the star (e.g. magnetic spots). Note that the rotational broadening is determined by contributions from a wide range of the area on the visible hemisphere, while the brightness modulation measures the rotation period at the latitude where spots evolve. For the Sun, it is well known that the spots migrate from  $\approx 30^\circ$  (Maunder 1904) toward the equator during their 11-year cycle, so that  $v \sin i$  and  $P_{\text{rot}}$  may not be sensitive to rotation of the same regions. This means that

the observed rotation frequency  $f_{\text{surf}}^{(1)}$  and  $f_{\text{surf}}^{(2)}$  may intrinsically differ from each other in case of significant latitudinal differential rotation. This point is further discussed in section 4.

The spectroscopic  $v \sin i$  of the analysed CoRoT stars has been measured by Bruntt (2009), while, except for HAT-P-7 and *Kepler*-25, the studied *Kepler* stars have been observed spectroscopically by Bruntt et al. (2012). Since Bruntt et al. (2012) do not provide uncertainties, we assumed here a typical precision of 10 per cent. Regarding HAT-P-7 and *Kepler*-25, we use values determined by Pál et al. (2008) and Marcy et al. (2014), respectively.

The surface rotation frequencies  $f_{\text{surf}}^{(2)}$  of the two CoRoT stars, HD 49933 and HD 181420 are from Benomar et al. (2009) and Barban et al. (2009), respectively, who have detected the low-frequency periodicity in the power spectrum. Note that alternative values were derived by using a stellar spot modelling technique in Mosser et al. (2009). These are in agreement with the surface rate used in this study (see Table A2). For *Kepler* stars, they are determined from rotation periods  $P_{\text{rot}}$ , which have been measured by García et al. (2014) based on the wavelet transform and on the analysis of the autocorrelation function of the light curve<sup>4</sup>. When the comparison is possible, their derived surface rotation is consistent with the rotation from Karoff et al. (2013). Note that  $f_{\text{surf}}^{(2)}$  cannot be evaluated for HAT-P-7 and *Kepler*-25 because they do not show detectable surface activity.

### 3.2 Internal rotation and stellar inclination

Asteroseismology of solar-like stars, in the present case, is based on the photometry of the luminosity variation. Because of its stochastic nature, each solar-like mode has a Lorentzian profile in the power spectrum (Harvey 1985). In that case, the stellar oscillations can be expressed as a sum of Lorentzians over  $n$ ,  $l$  and  $m$ ,

$$P(\nu) = \sum_{n,l} \sum_{m=-l}^l \frac{H_{n,l,m}}{1 + 4(\nu - \nu_{n,l,m})^2 / \Gamma_{n,l,m}^2}. \quad (6)$$

Here,  $\nu_{n,l,m}$  is given by equation (1), while  $H_{n,l,m}$  and  $\Gamma_{n,l,m}$  correspond to the mode height and width at half maximum, respectively.

The turbulent convection, which is the origin of acoustic modes, does not prefer any particular direction to others, so that the rotationally split modes with the same  $l$  and  $n$  are expected to have almost the same amplitudes. Due to a geometrical projection effect (Ballot, García & Lambert 2006; Gizon & Solanki 2003), in disk-integrated photometry, the height of the split modes depend on the stellar inclination angle  $i$  as  $H_{n,l,m} = \mathcal{E}_{l,m}(i)H_{n,l}$ . Here  $H_{n,l}$  is the intrinsic height for the mode, while  $\mathcal{E}_{l,m}(i)$  is the visibility of the  $m$ -components in the power spectrum,

$$\mathcal{E}_{l,m}(i) = \frac{(l - |m|)!}{(l + |m|)!} \left[ P_l^{|m|}(\cos i) \right]^2, \quad (7)$$

with  $P_l^{|m|}$  being the associated Legendre function. It is therefore possible to determine  $i$  from  $\mathcal{E}_{l,m}(i)$ . Several authors have already exploited that approach to measure the stellar inclination (e.g. Ballot et al. 2008; Benomar et al. 2009; Appourchaux et al. 2012; Chaplin et al. 2013; Benomar et al. 2014a; Lund et al. 2014).

In practice, the rotational splittings and the inclination angle are determined, together with the Lorentzian parameters, by

fitting the power spectrum of the light curve with the formula given by equation (6). Therefore, the precision on the rotation is limited by the correlation between the rotational splitting and of the stellar inclination. Note that the splitting is assumed constant over the observed range of modes in this analysis. As shown by Benomar et al. (2014a), the correlation problem is particularly important in slow rotators, because the  $2l + 1$   $m$ -components of the same order  $n$  and degree  $l$  are difficult to disentangle from each other. Contrary to heat driven pulsators, stochastically driven pulsators have an important intrinsic noise of stellar origin that renders mode pulsations hard to analyse and requires sophisticated statistical methods. Here, we use a Markov Chain Monte Carlo method (see e.g. Benomar, Appourchaux & Baudin 2009; Handberg & Campante 2011, for applications in asteroseismology). This allows us to evaluate the probability density function for the rotational splitting and stellar inclination, as well as their correlations. Note that part of studied stars have been analysed by Appourchaux et al. (2012) and Appourchaux et al. (2014), whose work focuses on mode frequencies, widths and heights. Stars of the current work in common with these studies are revisited here using the same data, but focusing on the extraction of the rotation and the stellar inclination angle.

### 3.3 Centrifugal distortion

In section 2.1, we have assumed that the internal rotation produces equal spacings in each multiplet of the power spectrum, as the first-order perturbation analysis due to the Coriolis force predicts. However, this cannot be fully justified if the second-order effect caused by the centrifugal force affects the pulsation modes significantly. Assuming uniform rotation, we can estimate the effects of the Coriolis and centrifugal forces by the two dimensionless parameters,  $\epsilon_1 = f/\nu$  and  $\epsilon_2 = (f/\nu_K)^2$ , respectively, in which  $f$  and  $\nu$  are the rotational and pulsational frequencies, respectively, and  $\nu_K = (2\pi)^{-1}(GMR^{-3})^{1/2}$  (e.g. Saio 1981).

These two parameters are related to the asymmetry of each multiplet by

$$\left| \left[ \nu_0 - \frac{\nu_m + \nu_{-m}}{2} \right] \left[ \frac{\nu_m - \nu_{-m}}{2m} \right]^{-1} \right| \sim \frac{\epsilon_2}{\epsilon_1} \quad (8)$$

for  $m \geq 1$ , where  $\nu_m$  represents the frequency of the component specified by the azimuthal order  $m$ . It is possible that the Coriolis and the centrifugal force are of the same order in some of the solar-like stars, which would induce an asymmetry of the multiplets in the power spectrum. Still, fitting such asymmetric structure with the symmetric formula should mainly introduce additional systematic errors in our estimates of the rotational splittings (and the stellar inclination), rather than lead to completely wrong values of them. In fact, the frequency difference,  $(\nu_m - \nu_{-m})/(2m)$ , which is equal to the rotational splitting, is not modified by the centrifugal distortion, but only changed by the third- and higher-order effects, which are negligibly small in all the stars. Moreover, if the asymmetry is significant, our analysis should suggest multiple different values of the rotational splittings. In the case of dipole modes, for example, we should find not only the correct value,  $(\nu_{m=1} - \nu_{m=-1})/2$ , but also two other different spacings (at most), one between  $m = 1$  and  $m = 0$  components, and the other between  $m = 0$  and  $m = -1$  components. Since most of the probability density functions, which are shown in Fig. A1, do not have such multiple-peak structure, we presume that the asymmetry is generally smaller than (or comparable to) the width of the main peak in the probability density functions.

<sup>4</sup> Using KADACS and PDC-MAP data, see García et al. (2011); Thompson et al. (2013).

### 3.4 Stellar models

In order to evaluate  $I_{\text{conv}}$  and  $I_{\text{rad}}$  in equation (3), it is necessary to determine the thickness of the convective and radiative zones. In addition, an estimate of the radius of each star is needed to evaluate the surface rotation rate based on the  $v \sin i$  measurements. All of these quantities are obtained by computing stellar models that simultaneously match non-seismic observables ( $T_{\text{eff}}$ ,  $\log g$  and  $[\text{Fe}/\text{H}]$ ) and seismic observables (mode frequencies). The used constraints, their source and our results are summarised in Table A1.

The best fitting models have been found using the ‘astero’ module of the Modules for Experiments in Stellar Astrophysics (MESA) evolutionary code (Paxton et al. 2011, 2013). Stellar models have been calculated assuming a fixed mixing-length parameter  $\alpha_{\text{MLT}} = 2.0$ . We have used OPAL opacities from Iglesias & Rogers (1996) and the solar composition (for the mixture of heavy elements) from Asplund et al. (2009). The initial hydrogen abundance has been fixed to  $X_0 = 0.7$ . No diffusion has been taken into account. Nuclear reactions have been set to include standard hydrogen and helium burning; the pp-chain and the CNO cycle in addition to the triple alpha reaction, which is the default setup of the MESA ‘astero’ module. We have utilised the NACRE compilation of nuclear reaction rates (Angulo et al. 1999) with the updates for  $^{14}\text{N}(p, \gamma)^{15}\text{O}$  and  $^{12}\text{C}(\alpha, \gamma)^{16}\text{O}$  reactions (Kunz et al. 2002; Formicola et al. 2004).

We have adopted the M. Schwarzschild treatment to define the boundary between the convective and radiative zones. Note that we do not take account of the convective overshooting, which we understand modifies the age of the stars, the position of the Base of the Convective Zone (BCZ) and the stellar radius to some extent. In order to assess the importance of this effect, we have computed models of HD 49933 (index 21), HD 181420 (index 22), *Kepler*-25 (index 19), and HAT-P-7 (index 20) including the overshoot. These models have shown that by neglecting the overshoot, the BCZ and the radius are changed by only a few per cent, at a level that does not significantly influence the inferred internal rotation rate ( $f_{\text{rad}}$ ). However, it can affect the age (and hence the central hydrogen abundance) by 25 per cent typically.

Eigenfrequencies have been calculated using ADIPLS (Christensen-Dalsgaard 2008), which assumes adiabaticity. We have applied surface effect corrections to the frequencies, following the method of Kjeldsen, Bedding & Christensen-Dalsgaard (2008). The search for the best fitting model has involved a simplex minimisation approach (Nelder & Mead 1965) using the  $\chi^2$  criteria, where the mass  $M$ , metallicity  $[\text{Fe}/\text{H}]$  and age are the free parameters of the fit.

## 4 RESULTS

The sensitivity of the average rotational splitting to the rotation rate within the radiative zone is estimated to be  $\langle I_{\text{rad}} \rangle = 32\text{--}64$  per cent (the full list is given in Table A1 in appendix A). This range is consistent with what is reported in Figs 1(b) and 2(b). Using the uncertainty in the radius, we estimate the error in  $\langle I_{\text{rad}} \rangle$  to be approximately 4 per cent. This is used to calculate the total uncertainty in the average rotation rate of the radiative zone.

Fig. 3 shows the HR diagram of our samples (blue dots). The numbers identify the stars and correspond to those in the index column of Tables A1 and A2. Luminosities of these models are determined so that the models fit both the non-seismic

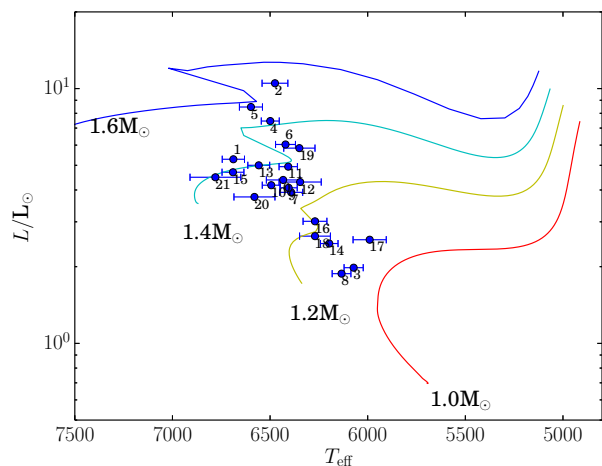


**Figure 3.** Best fitting models of the 22 analysed stars in the HR diagram. The numbers identify each of stars and correspond to those in the index column of Tables A1 and A2. These models have been computed with the MESA code so that they match both the non-seismic observables ( $T_{\text{eff}}$ ,  $\log g$  and  $[\text{Fe}/\text{H}]$ ) and the seismic observables (mode frequencies) simultaneously. Evolutionary tracks are for the solar metallicity.

and seismic observables, while the effective temperatures  $T_{\text{eff}}$  are those from spectroscopy. The coloured lines are evolutionary tracks with the adopted physics and for the solar metallicity. Our sample contains predominantly F stars — some of which have been extensively analysed for activity variations and magnetic cycles by Mathur et al. (2014) —, with masses spanning from  $\simeq 1.0 M_{\odot}$  to  $\simeq 1.6 M_{\odot}$ , an effective temperature  $5990 \text{ K} < T_{\text{eff}} < 6690 \text{ K}$  and a metallicity similar to the Sun. Table A1 provides more detailed information about the best fitting models of each star.

### 4.1 Mode identification

A fundamental step in asteroseismology is to fix the indices  $n$  (radial order),  $l$  (degree) and  $m$  (azimuthal order) of each observed mode. This is generally called mode identification. Eigenmodes of cool G type stars among our sample can easily be identified (at least for  $l$ ) by visual inspection of the so-called échelle diagram (Grec, Fossat & Pomerantz 1983). Furthermore, the relative height of each low-degree mode in the power spectrum (mode visibility  $V_l$  of degrees  $l$ , defined by  $H_{n,l} = V_l^2 H_{n,l=0}$ ) is mostly due to a geometrical effect, and therefore is nearly independent of the fundamental properties of the stars (Ballot, Barban & van’t Veer-Menneret 2011). This property is also used to identify modes in the star’s power spectrum.

However, in some cases, particularly for relatively hot stars, eigenmodes of the same parity (e.g.  $l = 0$  and  $l = 2$ ) are hard to disentangle from each other by visual inspection, mostly because the mode width at half maximum [see equation (6) for its definition] is of the same order as the frequency spacing between the modes. In such a case, the most likely mode identification relies on a statistical criteria such as the Bayes factor, between competitive solutions<sup>5</sup>

<sup>5</sup> There are actually only two possible solutions in the case of main sequence solar-like stars. Readers are recommended to refer to the papers cited above for additional explanations.

(Benomar, Appourchaux & Baudin 2009; Benomar et al. 2009; Appourchaux et al. 2012; Corsaro & De Ridder 2014). This problem of mode identification is actually recurrent in F stars and was first encountered in the CoRoT star HD 49933 (Appourchaux et al. 2008). In this paper, the mode identification of *Kepler* stars is based on Appourchaux et al. (2012), which used the methods discussed above. As for HD 49933 (index 21) and HD 181420 (index 22), the identification relied on the Bayes factor. It is the same as in Benomar et al. (2009) for HD 49933, and corresponds to Scenario 1 of Barban et al. (2009), for HD 181420. These identifications are also found as the most likely by White et al. (2012), using an independent approach.

Interestingly, an incorrect mode identification of  $l$  will often lead to a disagreement between the spectroscopic  $v \sin i$  and the seismic  $v_{\text{seis}} \sin i = 2\pi R f_{\text{seis}} \sin i$  (see Table A2). Therefore, stars with indications of important disagreement should be carefully discussed. Here, we check that the mode identification is correct for KIC 9139163 (index 10) which is also discussed in section 4.6. We note that the modes of the same parity are disentangled and visible in the échelle diagram, with the expected mode visibilities. We therefore conclude that our current mode identification of  $l$  is correct for this star.

As for KIC 3424541 (index 3), the mode identification reported in Appourchaux et al. (2012) leads to the seismic  $v_{\text{seis}} \sin i = 12.1 \pm 2.3 \text{ km s}^{-1}$ , which is incompatible with the spectroscopic  $v \sin i = 29.8 \text{ km s}^{-1}$  from Bruntt et al. (2012). In order to check the mode identification, we have used the latest *Kepler* data (Q5 to Q17), computed the Bayes factor of the two possible solutions and found that it is not in favour of the identification of Appourchaux et al. (2012). Note that due to its relatively fast rotation this star has a rotational splitting of the same order as the frequency spacing between modes of degree  $l = 2$  and  $l = 0$ , while the stellar inclination is of  $\approx 90^\circ$ . In such a configuration, the mode identification is not obvious because the azimuthal order  $m = -1$  of the degree  $l = 1$  can easily be falsely identified as an  $l = 2$  multiplet, while the  $m = +1$  could be falsely identified as an  $l = 0$ . Note also that Appourchaux et al. (2012) used a Bayesian framework, but with a shorter dataset. The new identification, which has permuted  $l = 1$  and the pairs of  $l = 0, 2$ , leads to  $v_{\text{seis}} \sin i = 26.89^{+0.80}_{-0.84} \text{ km s}^{-1}$ . This new result is in agreement with the spectroscopic  $v \sin i$ . Additional information regarding the analysis of this star is available in appendix B.

## 4.2 Probability density functions

Fig. 4 shows the joint-probability density functions of the stellar inclination and the rotational splitting, derived from asteroseismology for KIC 7206837 (index 8), KIC 9139163 (index 10) and KIC 9206432 (index 11). We also estimate the projected equatorial radial velocity from this diagram by assuming uniform rotation;  $v_{\text{seis}} \sin i = 2\pi R f_{\text{seis}} \sin i$ . It also shows the surface rotation rates derived from two different kinds of observations as a function of the stellar inclination  $i$ ; one from the lightcurve modulation due to spots, and the other from the rotational broadening of spectroscopic absorption lines. KIC 7206837 is an example of good match between spectroscopic  $v \sin i$ ,  $P_{\text{rot}}$ ,  $f_{\text{seis}}$  and  $i$ , while KIC 9139163 and KIC 9206432 are examples of mismatch among the observables (candidates for significant radial differential rotation). The joint-probability density functions for all of the 22 stars are shown in Fig. A1 in appendix A.

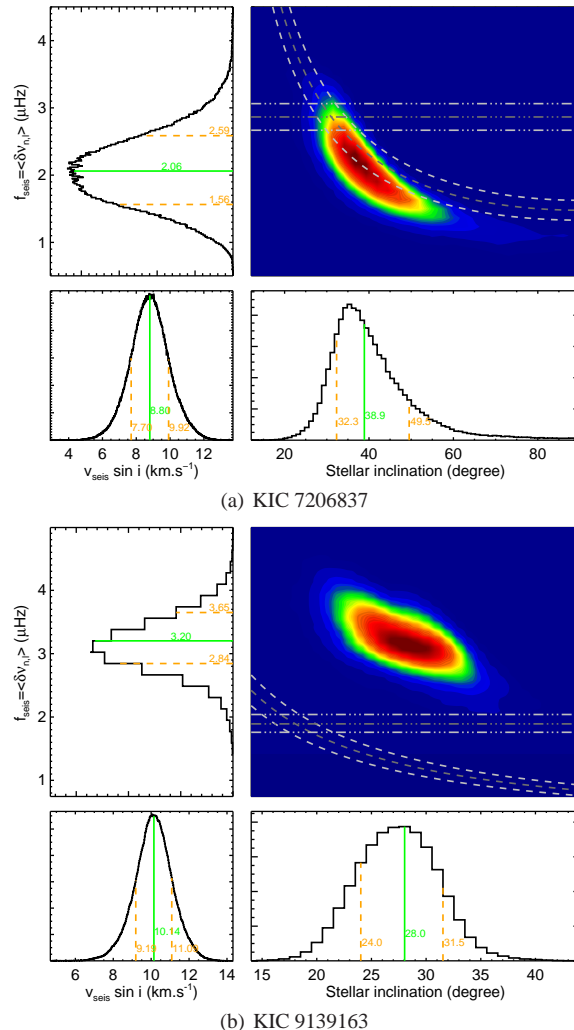


**Figure 4.** The colour maps show the correlation between the stellar internal rotation rates measured by the rotational splitting and the stellar inclination angles of three stars, on which superimposed are the surface rotation rates derived from the stellar spot (horizontal black dash-dotted lines) and the spectroscopic  $v \sin i$  (curved dotted lines). The confidence intervals are shown in grey. In case (a), the surface and internal rotation rates as well as the stellar inclination angle are all consistent with each other, which indicates a near solid-body rotation. In case (b), although the indicator of the surface rotation is consistent with the seismically derived stellar inclination, it is in disagreement with the internal rotation rate.

## 4.3 Surface rotation

As the surface rotation rate  $f_{\text{surf}}^{(1)}$  depends on  $v \sin i$ , the radius  $R$  and the stellar inclination  $i$ , it is useful to assess their respective contribution to the total uncertainty of  $f_{\text{surf}}^{(1)}$ . We estimate the uncertainties of the radius,  $v \sin i$  and the inclination  $i$  to be  $\delta R/R \simeq 1$  per cent,  $\delta v \sin i / v \sin i \lesssim 10$  per cent and  $\delta \sin i / \sin i \simeq 16$  per cent, respectively (see Table A2 in appendix A). Thus, the uncertainty of the stellar inclination is the dominant error term in  $f_{\text{surf}}^{(1)}$ , while the uncertainty in  $v \sin i$  is the second most important term. Meanwhile, as for our estimates of stellar radii listed in Table A1, the results of 91 per cent of the stars are compatible within  $2\sigma$  with

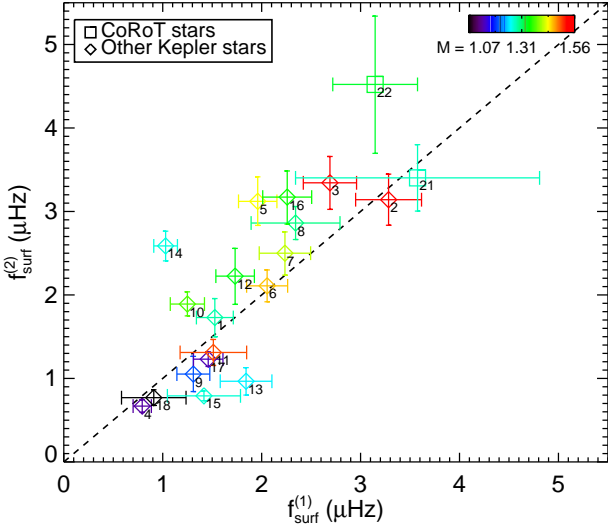


**Figure 5.** Comparison of the surface rotation rates estimated from (1) the rotational broadening of spectroscopic absorption lines,  $f_{\text{surf}}^{(1)}$ , and (2) the lightcurve modulation due to spots,  $f_{\text{surf}}^{(2)}$ . Colours show the mass of stars, while the black dotted line shows a one-to-one relation. The indices for the stars correspond to those in the first columns of Tables A1 and A2.

the estimates made by Metcalfe et al. (2014)<sup>6</sup>. This fraction drops to 72 per cent when comparing with stellar radii derived from the scaling relation that is calibrated by the Sun (Kjeldsen & Bedding 1995). Still, compatibility at  $3\sigma$  is kept— see further discussions in Mosser et al. (2013) —. Even if we consider a  $3\sigma$  uncertainty in the radius, the main error sources remain the stellar inclination and  $v \sin i$ .

Fig. 5 compares the two independent estimates of the surface rotation rates,  $f_{\text{surf}}^{(1)}$  and  $f_{\text{surf}}^{(2)}$ , which have been derived from the spectroscopic  $v \sin i$  and the lightcurve modulation due to surface structures, respectively. Although they are overall consistent with each other, some stars deviate from a one-to-one relation by approximately a factor of two. This could be (1) due to systematic errors in the spectroscopic  $v \sin i$ , (2) because multiple spot clusters appear at the same time at the surface of the stars, whereas the spot method is accurate only if one main structure exists, or (3) due to an intrinsic difference between the two estimates that originates from a latitudinal differential rotation. When small, the spectroscopic  $v \sin i$  can be poorly estimated because of the growing contribution of the microturbulence and macroturbulence relative to the actual rotational broadening of spectral lines. Microturbulence is of the order of one kilometre per second (e.g. Bruntt 2009; Doyle et al. 2014), *i.e.* significantly smaller than our  $v \sin i$  and is not expected to be a major source of bias. However, macroturbulence increases with the effective temperature (Valenti & Fischer 2005), and reaches  $4\text{--}8 \text{ km s}^{-1}$  in the case of F stars. As macroturbulence broadens the spectral lines, neglecting it overestimates  $v \sin i$ . This could explain that Fig. 5 shows a group of stars, such as KIC 10162436 (index 13) and KIC 10454113 (index 15), that lie below a one-to-one relation, but cannot explain the population of stars with  $f_{\text{surf}}^{(2)} \gg f_{\text{surf}}^{(1)}$  such as KIC 6508366 (index 5) and KIC

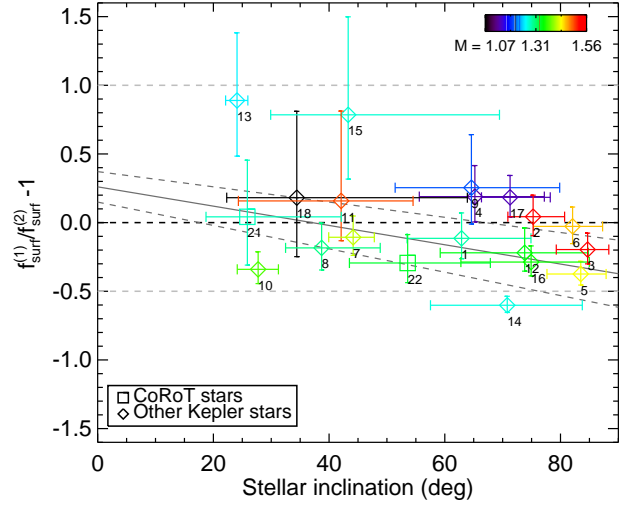


**Figure 6.** Ratio of the surface rotation rates deduced from two different kinds of observational data (one from the rotational broadening of spectral lines and the other from the lightcurve modulation due to spots) as a function of the stellar inclination. The indices for the stars correspond to those in the first columns of Tables A1 and A2. The linear fit that includes all stars –case (a)– is shown in dark gray. The best fit is the solid line, uncertainties at  $1\sigma$  are the dotted lines.

10355856 (index 14). However, we remark that these stars are seen from latitude near the equator ( $60^\circ < i < 90^\circ$ ), where most stellar spots are expected to emerge. Therefore, the important discrepancy between  $f_{\text{surf}}^{(1)}$  and  $f_{\text{surf}}^{(2)}$  could be due to the presence of multiple spots.

A latitudinal differential rotation may also lead to discrepancies between  $f_{\text{surf}}^{(1)}$  and  $f_{\text{surf}}^{(2)}$ . To estimate this, we looked at the ratio  $f_{\text{surf}}^{(1)}/f_{\text{surf}}^{(2)}$  as a function of the stellar inclination  $i$  (Fig. 6), which exhibits a trend. To assess its significance, we fitted a linear function  $f_{\text{surf}}^{(1)}/f_{\text{surf}}^{(2)} = a + bi$ , in three different situations,

- (a) with all observed stars. We obtain  $a = 0.26 \pm 0.12$  and  $b = 0.0015 \pm 0.008$ ,
- (b) excluding the star which shows the most extreme difference (star 14). We obtain  $a = -0.085 \pm 0.15$  and  $b = 0.001 \pm 0.003$ ,
- (c) excluding the three most extreme stars (star 13,14,15). We obtain  $a = -0.18 \pm 0.15$  and  $b = 0.000 \pm 0.003$ .

While case (a) indicates a significant slope (see also Fig. 6), case (b) and (c) show that the fit result strongly depends on a few extreme observations. We conclude that our measures do not strongly indicate evidences of a trend with  $i$  that could explain discrepancies described above. Further study on a larger sample, that better accounts for the macroturbulence is required before drawing firm conclusions on the latitudinal differential rotation. In any case, possible biases in  $v \sin i$  are expected to be less important than those in  $P_{\text{rot}}$ , and in the following, we choose to  $f_{\text{surf}}^{(1)}$  for the indicator of the surface rotation.

#### 4.4 Comparison between internal and surface rotation

Fig. 7 compares  $f_{\text{surf}}^{(1)}$  with the seismically obtained rotation rates  $f_{\text{seis}}$ . For reference, the Sun is also shown. The solar values of the rotational splitting for  $l = 1$  and  $l = 2$  with  $14 < n < 23$  were taken from Toutain (2001). We obtained their average of  $\langle \delta\nu_{nl} \rangle_{\odot} = 0.370 \pm 0.007 \mu\text{Hz}$ . The surface velocity is calcu-

<sup>6</sup> They modelled all *Kepler* stars of our sample except *Kepler*-25 and HAT-P-7, by taking account of more physical effects than our models, such as the overshooting and the diffusion.



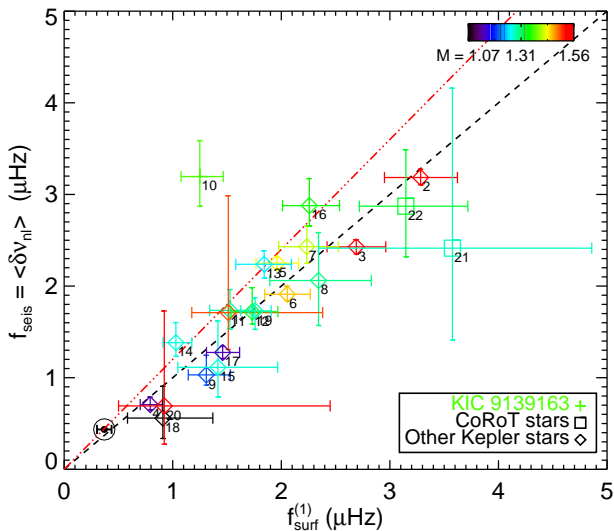


**Figure 7.** Rotational splittings versus surface rotation rates measured using the spectroscopic  $v \sin i$  for sampled stars. The solar symbol near the lower left corner indicates the Sun. The numbers attached to the stars correspond to those in the first columns of Tables A1 and A2. The ratios of these two quantities are mostly close to unity, implying that there is no significant radial differential rotation in most cases. The dashed triple-dotted line represents the expected positions of ZAMS models that assume local conservation of angular momentum in the radiative layers and constant rotation rates in the convection zone.

lated for the Sun-as-a-star, using the solar  $v_{\odot} \sin i_{\odot} = 1.6 \pm 0.3 \text{ km s}^{-1}$  from Pavlenko et al. (2012) and adopting  $R_{\odot} = 6.96 \times 10^5 \text{ km}$ . The ecliptic plane is inclined from the solar equatorial plane by approximately  $7^{\circ}$ , which means that  $\sin i_{\odot}$  can be different from 1 by 0.8 per cent at most. In Fig. 7,  $f_{\text{surf}}^{(1)}$  and  $f_{\text{seis}}$  are in good agreement, which already suggests that there is not a significant radial differential rotation in most cases. We thus confirm that nearly uniform rotation, which has been well established in the case of the Sun, extends to the faster rotating main-sequence stars with similar masses. However, we note that KIC 9139163 (index 10) depart significantly from the one-to-one relation, indicating that it seems to have faster-than-surface interior rotation.

In order to discuss the implication of this result, evolution of the rotation profiles of 1.2 and 1.5  $M_{\odot}$  stellar models with the solar composition has been calculated (Saio, private communication) from the (pre-main-sequence) Hayashi phase to the Zero-Age Main-Sequence (ZAMS) stage, with the following assumptions: (1) rotation rates are slow enough to have negligible effects on the structure, which keeps spherical symmetry, (2) total angular momentum is conserved (no addition to and no removal from the surface layers are considered), (3) the rotation profiles are functions of only radius, (4) angular momentum is locally conserved in the radiative zone and (5) it is redistributed instantaneously in the convection zone to establish a constant rotation rate (a limiting case of the efficient transport) with the total angular momentum of the zone fixed. Note that point (5) leads to uniform initial rotation profiles, because the models are fully convective in the Hayashi phase.

As the models evolve towards the ZAMS, the central mass concentration gets higher, which results in spin-up of the central part, whereas the rotation rate in the envelope augments more weakly. Consequently, the ratio between the central and surface rotation rates reaches about 2.5 (2.7) for the 1.2 (1.5)  $M_{\odot}$  model. Note that this ratio is independent of the initial rotation rate itself.

By substituting the calculated rotation profiles of the ZAMS models into equation (2), we have computed the average rotational splittings normalised by the surface rotation rate over all modes with  $l = 1, 2$  and  $n = 10\text{--}25$ . The resultant ratios are equal to 1.22 and 1.24 for the 1.2 and 1.5  $M_{\odot}$  models, respectively, which suggest that the ratio increases as a function of mass very mildly (at least in the range that we discuss in the present analysis). To take account of the smallest mass in our sample ( $\sim 1.0 M_{\odot}$ ), a common ratio of 1.2 is adopted for the ZAMS models between 1.0 and 1.6  $M_{\odot}$ . Fig. 7 shows a dashed triple-dotted line with this value of slope. During the subsequent evolution of the models after ZAMS, the central mass condensation continues, leading to an increase of the ratio as the models age. The line thus indicates the lower limit of the ratio that main-sequence stars in the mass range under consideration would have, if angular momentum were locally conserved in the radiative layers and fully redistributed in the convection zone to realise a constant rotation rate. Therefore, the stars that are found below the line in the figure provide clear evidence that angular momentum has been transported inside the radiative zone and/or between the radiative and convective zones of these stars. With a  $1\sigma$  confidence interval, the number of such stars is equal to 13 (those with indices 2, 3, 4, 6, 8, 9, 12, 15, 17, 18, 19, 21 and 22). At the  $2\sigma$  level<sup>7</sup>, it still remains 10 stars (2, 3, 4, 6, 9, 15, 17, 18, 19, 22).<sup>8</sup> Because the same physical process should operate in the same physical conditions, we presume that angular momentum is efficiently transported inside solar-like stars in general. Note that the magnetic braking of the surface layers, which is supposed to be effective for low-mass stars in our sample (Kraft 1967), is expected to increase the ratio of the rotation rates between the interior and the surface. The stars that have  $\sim 1.3 M_{\odot}$  or below, and found on or above the line on the figure (those with indices 10, 13, 14 and 16) could reflect a significant effect of this mechanism.

#### 4.5 Interpretation based on the simple two-layer model

To quantify the level of radial differential rotation in a different way, we evaluated the ratio  $\langle f_{\text{rad}}^{(1)} \rangle / f_{\text{surf}}^{(1)}$  based on equation (5). Fig. 8 shows that if we pickup randomly a solar-like star of our sample, there is 68 per cent probability that it has a rotation rate in the radiative zone not greater by 54 per cent and not slower by 41 per cent than the surface. Individually, the radial differential rotation does not exceed a factor of two, except for KIC 9139163 (index 10). Although it is in principle possible to obtain negative rotation rates, the observables do not provide us with enough information to distinguish the direction of rotation. Therefore, we exclude the possibility of opposite rotation rates (dashed area in Fig. 8)

#### 4.6 Particular cases of KIC 9139163 and KIC 9206432

In this section, we further discuss the case KIC 9139163 and KIC 9206432, which were more thoroughly analysed than other stars.

<sup>7</sup> The calculation has been done using the probability density functions and thus account for the skewness of the distributions.

<sup>8</sup> However, the values of  $v \sin i$  of stars with indices 4 and 18 are below  $5 \text{ km s}^{-1}$ , so that the contribution of macroturbulence could possibly be more significant than the estimated uncertainties.

4.6.1 *KIC 9139163*

Our analysis of KIC 9139163 leads to values of spectroscopic  $v \sin i$  which are less than half as small as the seismic  $v_{\text{seis}} \sin i$ . The spectroscopy gives  $v \sin i = 4.00 \text{ km s}^{-1}$ , while the seismically derived value is  $v_{\text{seis}} \sin i = 10.15 \pm 0.95 \text{ km s}^{-1}$ . It does not seem that these meaningful differences can be fully explained by only the known biases in the spectroscopic  $v \sin i$  (see section 4.3). The surface rotation derived from spots still appears to indicate an important radial differential rotation, as  $f_{\text{rad}}^{(2)}/f_{\text{surf}}^{(2)} \simeq 2.3$  (instead of  $f_{\text{rad}}^{(1)}/f_{\text{surf}}^{(1)} \simeq 3.8$ ). In general, the mode identification of oscillations in F stars is harder than in G stars, and one might think that this could also be a source of discrepancy. However, that latter possibility is ruled out for this star (see section 4.1 for further discussion).

A careful review of the assumptions in our analysis revealed that the centrifugal distortion may explain the apparent discrepancy. In our analysis and as discussed in section 3.3, this was neglected so that the internal rotation is assumed to produce equal spacings in each multiplet of the power spectrum. However, by comparing the two parameters for a representative frequency of the star, it is found that they can be of the same order. We thus performed a new analysis that includes the centrifugal distortion, in similar fashion as it has been done for *Kepler*-410A by Van Eylen et al. (2014). We found that the centrifugal force effect is negligible and did not modify neither the splitting nor the stellar inclination<sup>9</sup>. We conclude that second order effects on the splitting are not the cause of the discrepancy between the surface rotation and the internal rotation.

Mode visibilities  $V_{l=1}^2$  and  $V_{l=2}^2$  which were considered as free parameters may also modify the results as an important correlation with the splitting may exist. This is because in hot stars, modes of degree  $l = 0$  and  $l = 2$  (see section 4.1), potentially overlap. However, a new analysis that fixes them to the expected visibilities  $V_{l=1}^2 = 1.5$  and  $V_{l=2}^2 = 0.5$  did not modify neither the splitting nor the inclination.

4.6.2 *KIC 9206432*

For this star, the mode identification is not evident from the echelle diagram and requires to rely on the Bayes factor, which is in favour of the mode identification from Appourchaux et al. (2012). Furthermore, the same identification is obtained using the empirical approach from White et al. (2012). Note also that the less likely mode identification gives  $i \simeq 55^\circ$  and  $f_{\text{seis}} \simeq 3 \mu\text{Hz}$ , which leads to a great discrepancy between spectroscopic and seismic  $v \sin i$ . We thus assume in the following, that correct mode identification is the one already presented in Appourchaux et al. (2012).

The inferred rotation for the most likely mode identification is very sensitive to the fit assumptions. Our analyses revealed that the stellar inclination is relatively low, so that the  $m \neq 0$  components of the degree  $l = 1$  do not have a significant power and do not provide an accurate constraint on the rotational splitting. Furthermore, the modes of degree  $l = 0$  and  $l = 2$  overlap significantly, so that these can hardly be disentangled. Without tight constraints on the mode visibilities (i.e. when mode visibilities are free parameters) we noticed that the fit is unable to distinguish the small separation  $d_{02}$  from the rotational splitting  $\langle \delta\nu_{nl} \rangle$ . This leads to visibilities far greater than expected. We found

<sup>9</sup> We found  $\delta\nu_{nl} = 3.16_{-0.51}^{+0.56}$  and  $i = 23.6_{-2.8}^{+3.1}$ .

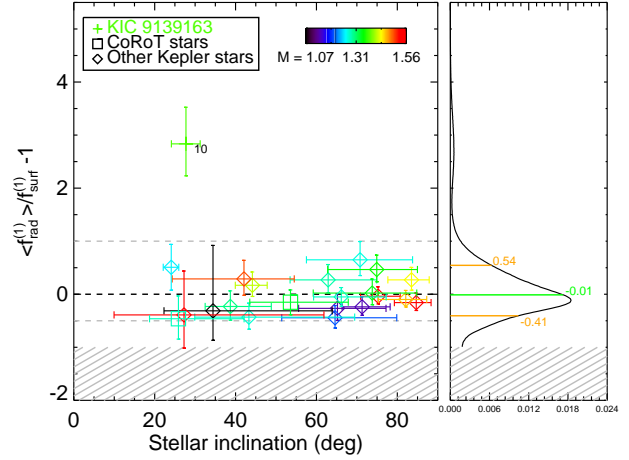


**Figure 8.** **Left.** Average radial differential rotation between the radiative zone and the surface as a function of the stellar inclination. Grey lines indicate a differential rotation of a factor of two. The dashed area indicate negative rotation rates. **Right.** Probability density function for  $\langle f_{\text{rad}}^{(1)} \rangle / f_{\text{surf}}^{(1)} - 1$  of the sampled stars. The median is shown in green, while orange lines indicate the confidence interval at  $1\sigma$ .

$V_{l=1}^2 = 2.2 \pm 0.3$  and  $V_{l=2}^2 = 1.3 \pm 0.2$  instead of  $V_{l=1}^2 = 1.5$  and  $V_{l=2}^2 = 0.5$ . It also gives a biased rotational splitting which leads to an apparent disagreement between spectroscopic and seismic, as  $v \sin i = 6.70 \text{ km s}^{-1}$  while  $v_{\text{seis}} \sin i = 13.66_{-1.64}^{+0.93} \text{ km s}^{-1}$ .

Fixing  $V_{l=1}^2 = 1.5$  and  $V_{l=2}^2 = 0.5$ , reduce the degeneracy of solutions and gives a better agreement ( $v_{\text{seis}} \sin i = 8.21_{-1.17}^{+1.30} \text{ km s}^{-1}$ ). We also evaluated the influence of  $l = 3$  modes in our analysis (with all visibilities fixed and  $V_{l=3}^2 = 0.07$ ) and found an even better agreement ( $v_{\text{seis}} \sin i = 7.77_{-0.98}^{+0.99} \text{ km s}^{-1}$ ).

Thus in that particular case, it is necessary to provide strong constraints on the mode visibilities in order to disentangle the power associated to the  $l = 0$  from its neighbour  $l = 2$  and consequently, to accurately measure the rotational splitting. Note that in the following, we provide the results of the fit with fixed visibilities and that includes  $l = 3$  because the calculation of the Bayes ratio indicates that these are statistically significant<sup>10</sup>

## 5 DISCUSSION

In the following, we further discuss the implications of our results.

## 5.1 Sample selection

The ensemble of 22 stars analysed in this paper are selected by the following criteria: (1) they are not known to be members of close binary systems; (2) they must show solar-like oscillations; (3) they must have a surface rotation velocity of at least a few kilometres per second to have accurate  $v \sin i$ ; (4) they are preferably hot solar-like stars (F stars), so that they have a thin convective envelope, a condition that improves the accuracy on the measured rotation rate of the radiative zone. While (1) is an important criteria for having reliable spectroscopy, our sample representativity for the ensemble of solar-like population has to be discussed for (2, 3, 4). Among the initial

<sup>10</sup> By comparing the model that includes  $l = 3$  with the one that does not, we found a Bayes ratio of  $\approx 70$ , which corresponds to a probability of 98% in favour of the model with  $l = 3$ .

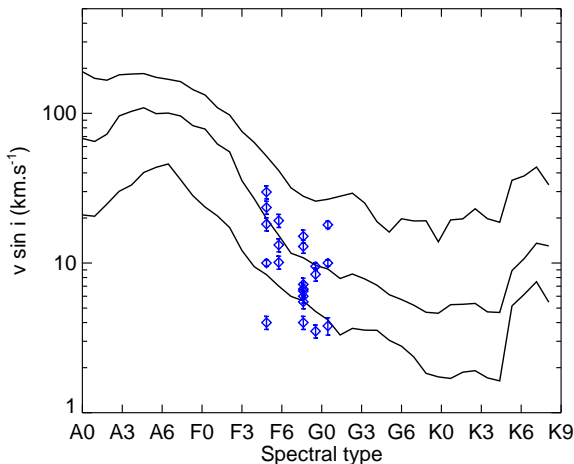


**Figure 9.** Comparison of the  $v \sin i$  in our sample (blue diamonds) with  $v \sin i$  from the catalog of Glebocki & Gnacinski (2005). Upper and lower lines indicate the  $1\sigma$  interval of catalog population, The middle line is the median.

2000 stars selected for asteroseismic observation (in short-cadence mode) in the *Kepler* field, only 500 showed sufficiently low activity to enable the detection of solar-like oscillations (Chaplin et al. 2011). This may indicate that we are biased towards low-activity stars. Furthermore, the least massive and cooler solar-like pulsators are not represented in our sample mostly because of their weak, hard to detect, pulsations. Yet, we hypothesise that because the same physical processes should operate in all solar-like pulsators, our results might be extrapolated to cooler or more active stars. One may also argue that our sample is not representative in terms of  $v \sin i$ . However no evident bias can be seen in Fig. 9, which compares the spectroscopic  $v \sin i$  of our sample (blue symbols) with a catalog of  $v \sin i$  for 28179 stars (Glebocki & Gnacinski 2005). In this catalog, we only selected stars of K9 to A0 type for which uncertainties were provided (over 9000 stars). Thus we think that our conclusion that most stars slightly more massive than the Sun, rotate nearly uniformly is valid for most of solar-like stars. Further analysis, based on a larger and homogeneous sample of stars would help to confirm this.

## 5.2 Main results and their implications

We have demonstrated that, for most of the 22 main-sequence stars in our sample, which have masses between  $1.0$  and  $1.6 M_{\odot}$ , the surface rotation rate and the average rotation rate of the nearly whole star (except for the central 15 per cent region in radius) are almost consistent with each other. The difference between the two rates is so small for 10 stars that the simple evolutionary models without transport of angular momentum inside the radiative zone and between the radiative and convective zones are clearly rejected (see Fig. 7). Expecting that the physical mechanism is universal, it is inferred that efficient transport of angular momentum generally occurs in solar-like stars. Assuming uniform rotation in each of the convective envelope and the radiative zone, it has been found for 21 out of the 22 stars that the rotation rates of the two zones do not differ by more than a factor of two.

As gyrochronology suggests that younger stars rotate faster than older stars, we attempted to identify signs of decrease of rotation rate in the interior ( $f_{\text{rad}}^{(1)}$ ) by using two age indicators,

(a) the hydrogen central abundance  $X_c$  from the models.

(b) the seismic observed ratio between the small separation  $d_{02} = \nu_{n-1,l=2} - \nu_{n,l=0}$  and the frequency spacing between consecutive modes of same degree  $\Delta\nu = \nu_{n,l} - \nu_{n-1,l}$ .

As shown by Fig. 10(a), the models of the stars have various ages since the core-hydrogen abundance  $X_c$  spans between  $\sim 0.01$  and  $\sim 0.54$ , leading to  $X_c/X_0 \sim 1$  per cent at the lower limit and  $X_c/X_0 \sim 78$  per cent at the upper limit.<sup>11</sup> No trend suggesting a change of rotation rate along evolution is visible. This indicates that an angular momentum transport mechanism is efficient from the early main-sequence stage, and possibly even since the pre-main-sequence phase.

Along evolution, models indicate that  $d_{02}/\Delta\nu$  decreases, which might be associated to a decrease of rotation rate in low-mass stars with a significant magnetic braking. Instead, in Fig. 10(b), the rotation appear to increase with  $d_{02}/\Delta\nu$ . Actually, because this indicator also decreases as the mass increase, the seen trend is mostly due to a mass-rotation relation.

Interestingly, only one star, KIC 9139163 (index 10) seems to have a significantly faster rotation rate in the interior than the surface. We note that this star is among the youngest and massive stars in our sample, which may indicate that the near solid body rotation has not been established in these stars yet. The study of a larger sample, with possibly younger stars, may help to better evaluate when the angular momentum transfer mechanism becomes effective and to derive timescales of such a process. On the other hand, additional analysis of the current candidate for a large radial differential rotation is also required. For example, new high resolution spectroscopic observations would be useful to confirm measures from Bruntt et al. (2012) and to assess the uncertainties in  $v \sin i$ . KIC 9139163 could be an interesting case for the study of the differential rotation because it shows a large contrast between interior and surface rotation. However we stress that due to the low stellar inclination ( $\simeq 20^\circ$ , which implies that the power of  $|m| > 0$  relative to the  $m = 0$  is only of  $\simeq 15\%$  for  $l = 1$  modes and  $\simeq 35\%$  for  $l = 2$  modes), our result could be very sensitive to the noise realisation and therefore, on the noise background model. This issue has also been discussed by Corsaro & De Ridder (2014) for that star. Thus, further studies are certainly required to confirm the unusually fast interior rotation of KIC 9139163.

Because the mass range of our sample between  $1.0$  and  $1.6 M_{\odot}$  is about the same as that of six subgiants and young red giants analysed by Deheuvels et al. (2014), the comparison of the two studies allows us to examine the evolution of internal rotation of stars in this mass range during the post-main-sequence stage. Since our analysis has demonstrated that these stars rotate almost uniformly in the main-sequence stage, the contrast (of about factor 60 at most) in the rotation rate between the core and the envelope detected in the subgiants and young red giants should be understood as the outcome of the competition between the two effects, the efficient angular momentum transport and the expansion of the envelope after the main-sequence phase. This picture was already suggested by Deheuvels et al. (2012), with the assumption of uniform rotation at the end of the main-sequence stage. The present analysis strongly supports their assumption.

<sup>11</sup>  $X_0 = 0.7$  is the initial hydrogen abundance (see section 3.4).

### 5.3 Implication in the problem of misaligned exoplanet systems

Some of exoplanet systems show significant misalignment between the rotation axis of the host star and the normal of the orbital plane. It is even claimed that some exoplanets orbit in the opposite direction to the rotation of the host star (e.g. Xue et al. 2014). In order to explain this phenomenon, Rogers, Lin & Lau (2012) proposed a hypothesis that the near-surface layers of the host star rotate in the opposite direction to the rest of the star, being caused by the angular momentum transport by gravity waves that are generated at the outer boundary of the convective core. Since our analysis simply assumes that all layers of the stars rotate in the same direction about a common axis, the sign change of the rotation rate cannot be measured directly by our analysis. However, if such reversal occurs, it should be still detectable by the analysis in this paper as a large difference between the surface rotation rate and the average rotation rate over the large range of the star (the rotational splitting). The fact that most of the stars in our sample, including those with known exoplanets (HAT-P-7 and *Kepler-25*), rotate almost uniformly (see Fig. 7) clearly contradicts such reversal. Thus, the present analysis does not support the hypothesis proposed by Rogers, Lin & Lau (2012) as a general picture of F type main-sequence stars.

### 5.4 Characteristics of the method

Our method of measuring the rotation rates of solar-like pulsators is based on (1) usage of asteroseismic analysis and (2) combination with spectroscopic observations. In the following, these two points are explained within the context of the internal rotation measurements in asteroseismology.

The first point is justified by the fact that the rotational splittings detected in the main-sequence solar-like pulsators are sensitive to the rotation not only in the convective envelope but also in the radiative zone. Lund, Miesch & Christensen-Dalsgaard (2014a) examined the rotation kernels of high-order and low-degree modes of a solar-mass main-sequence stellar model, taking account of dependence on not only radius but also co-latitude. They wrote in section 2.1, “It is clear for all these modes that the kernels are mainly sampling the outer parts of the star”. But this statement should be accepted with great care for general solar-like stars. While the contribution from the radiative zone amounts to about 37 per cent in their model (Lund, Miesch & Christensen-Dalsgaard 2014b), the value can rise to more than 50 per cent for more massive solar-like stars, as demonstrated by Figs 1(b) and 2(b) of this paper. We understand that this is mainly because the convection envelope is thinner (in fractional radius) for more massive stars. The non-negligible contribution of the radiative interior means that the rotational splittings observed in solar-like stars also contain a considerable amount of information about the rotation in the radiative zone.

The second point reflects that it is difficult to distinguish the rotation rates between the radiative and convective zones based only on asteroseismic analysis. This is because the observed eigenmodes of each star have very similar rotation kernels to each other, as shown in Figs 1 and 2, and therefore all of the rotational splittings provide almost the same weighted average of the internal rotation rates. This has been known for a long time (e.g. Aerts, Christensen-Dalsgaard & Kurtz 2010) and confirmed by recent space-based observations, for which only the average rotational splitting within the range of observed modes is robustly measured (e.g. Appourchaux et al. 2008; Ballot, Barban & van’t Veer-Menneret 2011; Chaplin et al. 2013).

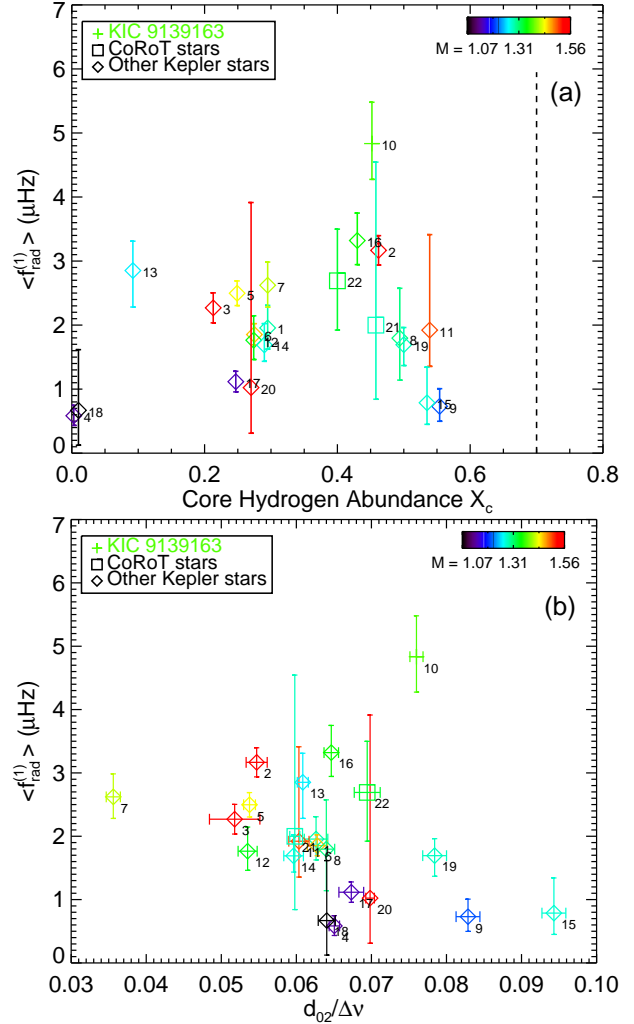


**Figure 10.** Internal rotation as a function two age indicators: (a) the core hydrogen abundance  $X_c$  derived from stellar modelling and (b) the reduced small separation  $d_{02}/\Delta\nu$ . In (a), the vertical dot line indicate the initial hydrogen abundance. Models do not account for overshoot which can modify  $X_c$  by 25 per cent. Selected stars cover a large part of the main sequence, but no evident slow down of the interior is observed along evolution. The trend seen in (b) indicate a stellar mass-rotation relation. .

Recently, Nielsen et al. (2014) were unsuccessful in detecting variations of the rotational splittings in *Kepler* stars. Therefore, an independent source of information is required to examine radial dependence of the rotation rate. For this purpose, we have exploited the surface rotation rate measured by the spectroscopic  $v \sin i$  combined with the average rotational splitting, allowing us to evaluate the degree of radial differential rotation.

### ACKNOWLEDGEMENTS

We thank NASA and CNES, as well as the *Kepler* and CoRoT teams for their revolutionary data. We are grateful to Enrico Corsaro, Benoit Mosser and Thierry Appourchaux for their useful comments. We express our gratitude to Hideyuki Saio for calculating the rotation profiles of evolutionary stellar models. O.B. is supported by Japan Society for Promotion of Science (JSPS) Fellowship for Research (No. 25-13316). M.T. thanks the support by JSPS

KAKENHI Grant Number 26400219. R.A.G. and T.C. thank the support of the CNES. We thank the referee for his/her comments that greatly improved the quality of the manuscript.

## REFERENCES

- Aerts C., Christensen-Dalsgaard J., Kurtz D. W., 2010, *Asteroseismology*
- Aerts C., Thoul A., Daszyńska J., Scuflaire R., Waelkens C., Dupret M. A., Niemczura E., Noels A., 2003, *Science*, 300, 1926
- Angulo C. et al., 1999, *Nuclear Physics A*, 656, 3
- Appourchaux T. et al., 2014, *A&A*, 566, A20
- Appourchaux T. et al., 2010, *A&A Rev.*, 18, 197
- Appourchaux T. et al., 2012, *A&A*, 543, A54
- Appourchaux T. et al., 2008, *A&A*, 488, 705
- Asplund M., Grevesse N., Sauval A. J., Scott P., 2009, *ARA&A*, 47, 481
- Baglin A., Auvergne M., Barge P., Deleuil M., Catala C., Michel E., Weiss W., COROT Team, 2006a, in *ESA Special Publication*, Vol. 1306, ESA Special Publication, Fridlund M., Baglin A., Lochard J., Conroy L., eds., p. 33
- Baglin A. et al., 2006b, in *COSPAR Meeting*, Vol. 36, 36th COSPAR Scientific Assembly, p. 3749
- Ballot J., Appourchaux T., Toutain T., Guittet M., 2008, *A&A*, 486, 867
- Ballot J., Barban C., van't Veer-Menneret C., 2011, *A&A*, 531, A124
- Ballot J., García R. A., Lambert P., 2006, *MNRAS*, 369, 1281
- Barban C. et al., 2009, *A&A*, 506, 51
- Beck P. G. et al., 2012, *Nature*, 481, 55
- Benomar O., Appourchaux T., Baudin F., 2009, *A&A*, 506, 15
- Benomar O. et al., 2009, *A&A*, 507, L13
- Benomar O. et al., 2014a, *ApJ*, 781, L29
- Benomar O., Masuda K., Shibahashi H., Suto Y., 2014b, *PASJ*, 66, 94
- Borucki W. J. et al., 2010, *Science*, 327, 977
- Bruntt H., 2009, *A&A*, 506, 235
- Bruntt H. et al., 2012, *MNRAS*, 423, 122
- Chaplin W. J. et al., 2014, *ApJS*, 210, 1
- Chaplin W. J. et al., 1999, *MNRAS*, 308, 405
- Chaplin W. J. et al., 2011, *Science*, 332, 213
- Chaplin W. J. et al., 2013, *ApJ*, 766, 101
- Christensen-Dalsgaard J., 2008, *Ap&SS*, 316, 113
- Christensen-Dalsgaard J. et al., 1996, *Science*, 272, 1286
- Corsaro E., De Ridder J., 2014, *A&A*, 571, A71
- Cowling T. G., Newing R. A., 1949, *ApJ*, 109, 149
- Davies G. R. et al., 2015, *MNRAS*, 446, 2959
- Deheuvels S. et al., 2014, *A&A*, 564, A27
- Deheuvels S. et al., 2012, *ApJ*, 756, 19
- Doyle A. P., Davies G. R., Smalley B., Chaplin W. J., Elsworth Y., 2014, *MNRAS*, 444, 3592
- Eff-Darwich A., Korzennik S. G., 2013, *Sol. Phys.*, 287, 43
- Elsworth Y., Howe R., Isaak G. R., McLeod C. P., Miller B. A., New R., Wheeler S. J., Gough D. O., 1995, *Nature*, 376, 669
- Formicola A. et al., 2004, *Physics Letters B*, 591, 61
- García R. A. et al., 2014, *A&A*, 572, A34
- García R. A. et al., 2004, *Sol. Phys.*, 220, 269
- García R. A. et al., 2011, *MNRAS*, 414, L6
- García R. A., Mathur S., Ballot J., 2008, *Sol. Phys.*, 251, 135
- García R. A., Mathur S., Ballot J., Eff-Darwich A., Jiménez-Reyes S. J., Korzennik S. G., 2008, *Sol. Phys.*, 251, 119
- Gizon L., Solanki S. K., 2003, *ApJ*, 589, 1009
- Glebocki R., Gnacinski P., 2005, *VizieR Online Data Catalog*, 3244, 0
- Grec G., Fossat E., Pomerantz M. A., 1983, *Sol. Phys.*, 82, 55
- Handberg R., Campante T. L., 2011, *A&A*, 527, A56
- Harvey J., 1985, *ESA SP*, 235, 199
- Iglesias C. A., Rogers F. J., 1996, *ApJ*, 464, 943
- Jeffreys H., 1961, *Theory of Probability*, 3rd edn. Oxford, Oxford, England
- Karoff C. et al., 2013, *MNRAS*, 433, 3227
- Kjeldsen H., Bedding T. R., 1995, *A&A*, 293, 87
- Kjeldsen H., Bedding T. R., Christensen-Dalsgaard J., 2008, *ApJ*, 683, L175
- Kraft R. P., 1967, *ApJ*, 150, 551
- Kunz R., Fey M., Jaeger M., Mayer A., Hammer J. W., Staudt G., Harissopulos S., Paradellis T., 2002, *ApJ*, 567, 643
- Kurtz D. W., Saio H., Takata M., Shibahashi H., Murphy S. J., Sekii T., 2014, *MNRAS*, 444, 102
- Lazrek M. et al., 1996, *Sol. Phys.*, 166, 1
- Ledoux P., 1951, *ApJ*, 114, 373
- Lund M. N. et al., 2014, *A&A*, 570, A54
- Lund M. N., Miesch M. S., Christensen-Dalsgaard J., 2014a, *ApJ*, 790, 121
- Lund M. N., Miesch M. S., Christensen-Dalsgaard J., 2014b, *ApJ*, 794, 96
- Marcy G. W. et al., 2014, *ApJS*, 210, 20
- Mathur S., Eff-Darwich A., García R. A., Turck-Chièze S., 2008, *A&A*, 484, 517
- Mathur S. et al., 2014, *A&A*, 562, A124
- Mathur S. et al., 2012, *ApJ*, 749, 152
- Maunder E. W., 1904, *MNRAS*, 64, 747
- Metcalfe T. S. et al., 2014, *ApJS*, 214, 27
- Mosser B., Baudin F., Lanza A. F., Hurlot J. C., Catala C., Baglin A., Auvergne M., 2009, *A&A*, 506, 245
- Mosser B. et al., 2013, *A&A*, 550, A126
- Nelder J. A., Mead R., 1965, *The Computer Journal*, 7, 308
- Nielsen M. B., Gizon L., Schunker H., Schou J., 2014, *A&A*, 568, L12
- Pál A. et al., 2008, *ApJ*, 680, 1450 (P08)
- Pamyatnykh A. A., Handler G., Dziembowski W. A., 2004, *MNRAS*, 350, 1022
- Pavlenko Y. V., Jenkins J. S., Jones H. R. A., Ivanyuk O., Pinfield D. J., 2012, *MNRAS*, 422, 542
- Paxton B., Bildsten L., Dotter A., Herwig F., Lesaffre P., Timmes F., 2011, *ApJS*, 192, 3
- Paxton B. et al., 2013, *ApJS*, 208, 4
- Pinsonneault M. H., An D., Molenda-Žakowicz J., Chaplin W. J., Metcalfe T. S., Bruntt H., 2012, *ApJS*, 199, 30
- Rogers T. M., Lin D. N. C., Lau H. H. B., 2012, *ApJ*, 758, L6
- Saio H., 1981, *ApJ*, 244, 299
- Saio H., Kurtz D. W., Takata M., Shibahashi H., Murphy S. J., Sekii T., Bedding T. R., 2015, *MNRAS*, 447, 3264
- Schou J. et al., 1998, *ApJ*, 505, 390
- Takata M., 2012, *PASJ*, 64, 66
- Thompson M. J., Christensen-Dalsgaard J., Miesch M. S., Toomre J., 2003, *ARA&A*, 41, 599
- Thompson S. E. et al., 2013, *Kepler data release 21 notes (ksci-19061-001)*
- Toutain T., 2001, *Sol. Phys.*, 200, 353
- Valenti J. A., Fischer D. A., 2005, *ApJS*, 159, 141
- Van Eylen V. et al., 2014, *ApJ*, 782, 14
- White T. R. et al., 2012, *ApJ*, 751, L36

Xue Y., Suto Y., Taruya A., Hirano T., Fujii Y., Masuda K., 2014,  
ApJ, 784, 66

**APPENDIX A: SUPPLEMENTARY CONTENTS FOR THE MAIN RESULTS**

Provided in this appendix are the following pieces of supplementary information about the analysis in the main part:

- (i) summary of the best fitting models in Table A1
- (ii) summary of the rotation rates at the surface and the radiative interior in Table A2
- (iii) joint-probability density functions in Fig. A1

**Table A1.** Parameters used to constrain models (left), those derived from models (middle) and mass/radius derived from the scaling relations (right). Effective temperatures are from Pinsonneault et al. (2012) and the other non-seismic constraints ([Fe/H] and  $\log g$ ) are from (i) Bruntt et al. (2012), (ii) Marcy et al. (2014), (iii) Pál et al. (2008) or (iv) Bruntt (2009). The uncertainty in  $\langle I_{\text{rad}} \rangle$  is about 4 per cent.

ind.	Name	Spec. type (MK)	Constraints				Results from models					Results from scal. rel.	
			$T_{\text{eff}}$ (K)	[Fe/H]	$\log g$ (cgs)	$L/L_{\odot}$	$M/M_{\odot}$	$R/R_{\odot}$	$X_c$	BCZ (frac. rad.)	$\langle I_{\text{rad}} \rangle$ (%)	$M/M_{\odot}$	$R/R_{\odot}$
1	KIC 1435467 <sup>(i)</sup>	F8	6433 ± 86	-0.11 ± 0.06	4.09 ± 0.08	4.38 ± 0.08	1.294 ± 0.039	1.686 ± 0.020	0.295	0.825	49.6	1.47 ± 0.04	1.75 ± 0.02
2	KIC 2837475 <sup>(i)</sup>	F5	6688 ± 57	-0.02 ± 0.06	4.16 ± 0.08	5.28 ± 0.03	1.553 ± 0.028	1.691 ± 0.020	0.462	0.902	62.8	1.51 ± 0.03	1.69 ± 0.01
3	KIC 3424541 <sup>(i)</sup>	G0	6475 ± 66	0.01 ± 0.06	3.82 ± 0.08	10.50 ± 0.20	1.556 ± 0.018	2.551 ± 0.026	0.213	0.875	58.1	1.80 ± 0.05	2.67 ± 0.02
4	KIC 6116048 <sup>(i)</sup>	F9	6072 ± 49	-0.24 ± 0.06	4.28 ± 0.08	1.98 ± 0.02	1.134 ± 0.027	1.274 ± 0.020	0.003	0.730	38.8	1.02 ± 0.02	1.23 ± 0.01
5	KIC 6508366 <sup>(i)</sup>	F6	6499 ± 46	-0.08 ± 0.06	3.94 ± 0.08	7.46 ± 0.08	1.436 ± 0.021	2.142 ± 0.020	0.249	0.864	55.9	1.61 ± 0.03	2.22 ± 0.02
6	KIC 6679371 <sup>(i)</sup>	F5	6598 ± 59	-0.13 ± 0.06	3.91 ± 0.08	8.47 ± 0.07	1.457 ± 0.021	2.167 ± 0.024	0.275	0.909	64.2	1.70 ± 0.04	2.30 ± 0.02
7	KIC 7103006 <sup>(i)</sup>	F8	6421 ± 51	0.05 ± 0.06	4.01 ± 0.08	6.04 ± 0.08	1.417 ± 0.025	1.941 ± 0.020	0.295	0.853	53.8	1.57 ± 0.03	2.00 ± 0.01
8	KIC 7206837 <sup>(i)</sup>	F8	6392 ± 59	0.14 ± 0.06	4.17 ± 0.08	3.92 ± 0.06	1.307 ± 0.027	1.562 ± 0.018	0.494	0.842	52.0	1.38 ± 0.03	1.59 ± 0.01
9	KIC 9139151 <sup>(i)</sup>	G0.5 <sup>(a)</sup>	6134 ± 48	0.11 ± 0.06	4.38 ± 0.08	1.88 ± 0.03	1.206 ± 0.077	1.170 ± 0.008	0.554	0.780	44.3	1.18 ± 0.02	1.16 ± 0.01
10	KIC 9139163 <sup>(i)</sup>	F8	6405 ± 44	0.15 ± 0.06	4.18 ± 0.08	4.08 ± 0.03	1.378 ± 0.028	1.561 ± 0.018	0.452	0.860	55.0	1.49 ± 0.03	1.60 ± 0.01
11	KIC 9206432 <sup>(i)</sup>	F8	6494 ± 46	0.23 ± 0.06	4.23 ± 0.08	4.18 ± 0.05	1.500 ± 0.050	1.551 ± 0.010	0.539	0.878	58.3	1.57 ± 0.03	1.59 ± 0.01
12	KIC 9812850 <sup>(i)</sup>	F8	6407 ± 47	-0.16 ± 0.06	4.05 ± 0.08	4.94 ± 0.07	1.343 ± 0.013	1.809 ± 0.010	0.274	0.822	49.1	1.40 ± 0.03	1.83 ± 0.01
13	KIC 10162436 <sup>(i)</sup>	F8	6346 ± 108	-0.08 ± 0.06	3.95 ± 0.08	4.30 ± 0.03	1.259 ± 0.015	1.971 ± 0.018	0.092	0.735	38.6	1.45 ± 0.05	2.05 ± 0.02
14	KIC 10355856 <sup>(i)</sup>	F5	6558 ± 56	-0.19 ± 0.06	4.08 ± 0.08	5.00 ± 0.05	1.273 ± 0.016	1.721 ± 0.018	0.290	0.862	55.3	1.43 ± 0.03	1.79 ± 0.01
15	KIC 10454113 <sup>(i)</sup>	F9	6197 ± 47	-0.06 ± 0.06	4.31 ± 0.08	2.47 ± 0.02	1.279 ± 0.024	1.285 ± 0.018	0.535	0.811	47.9	1.22 ± 0.02	1.27 ± 0.01
16	KIC 11253226 <sup>(i)</sup>	F5	6690 ± 56	-0.08 ± 0.06	4.16 ± 0.08	4.70 ± 0.07	1.355 ± 0.016	1.603 ± 0.023	0.430	0.893	60.7	1.69 ± 0.06	1.73 ± 0.02
17	KIC 12009504 <sup>(i)</sup>	F9	6230 ± 51	-0.09 ± 0.06	4.21 ± 0.08	3.01 ± 0.03	1.140 ± 0.074	1.386 ± 0.008	0.247	0.851	52.5	1.28 ± 0.03	1.45 ± 0.01
18	KIC 12258514 <sup>(i)</sup>	G0.5 <sup>(a)</sup>	5990 ± 85	0.04 ± 0.06	4.11 ± 0.08	2.55 ± 0.01	1.068 ± 0.034	1.543 ± 0.035	0.010	0.661	32.0	1.47 ± 0.04	1.64 ± 0.01
19	<i>Kepler-25</i> <sup>(ii)</sup>	F <sup>(b)</sup>	6270 ± 79	-0.04 ± 0.03	4.278 ± 0.03	2.64 ± 0.06	1.285 ± 0.036	1.348 ± 0.011	0.500	0.820	49.0	1.32 ± 0.03	1.36 ± 0.01
20	HAT-P-7 <sup>(iii)</sup>	F6	6350 ± 80	0.26 ± 0.08	4.070 ± 0.08	5.84 ± 0.05	1.540 ± 0.030	2.000 ± 0.009	0.270	0.870	57.4	1.48 ± 0.03	1.97 ± 0.01
21	HD 49933 <sup>(iv)</sup>	F8	6570 ± 60	-0.44 ± 0.03	4.28 ± 0.06	3.76 ± 0.08	1.287 ± 0.009	1.463 ± 0.006	0.458	0.880	58.3	1.34 ± 0.02	1.49 ± 0.01
22	HD 181420 <sup>(iv)</sup>	F6	6580 ± 105	0.00 ± 0.06	4.26 ± 0.06	4.49 ± 0.13	1.335 ± 0.010	1.622 ± 0.007	0.400	0.877	57.8	1.61 ± 0.05	1.73 ± 0.02

(a) Assumed as G0 in Fig. 9. (b) Assumed as F5 in Fig. 9.



**Table A2.** Rotation rates at the surface of the stars and in the radiative zone. The penultimate column indicates the length of the data set while the last column gives the first and last used *Kepler* data quarters.

index	Name	$f_{\text{seis}}$ ( $\mu\text{Hz}$ )	$i$ ( $^\circ$ )	$v_{\text{seis}} \sin i$ ( $\text{km s}^{-1}$ )	$v \sin i$ ( $\text{km s}^{-1}$ )	$P_{\text{rot}}$ (d)	$f_{\text{surf}}^{(1)}$ ( $\mu\text{Hz}$ )	$f_{\text{surf}}^{(2)}$ ( $\mu\text{Hz}$ )	$\langle f_{\text{rad}}^{(1)} \rangle$ ( $\mu\text{Hz}$ )	$\langle f_{\text{rad}}^{(2)} \rangle$ ( $\mu\text{Hz}$ )	Obs. duration (d)	Quarters
1	KIC 1435467	$1.73^{+0.23}_{-0.20}$	$62.90^{+12.60}_{-9.50}$	$11.29^{+0.67}_{-0.66}$	$10.00 \pm 1.00$	$6.68 \pm 0.89$	$1.53^{+0.22}_{-0.18}$	$1.73^{+0.23}_{-0.23}$	$1.96^{+0.35}_{-0.33}$	$1.76^{+0.50}_{-0.47}$	738	Q5-Q12
2	KIC 2837475	$3.19^{+0.08}_{-0.09}$	$75.40^{+5.60}_{-4.50}$	$22.79^{+0.59}_{-0.61}$	$23.50 \pm 2.35$	$3.68 \pm 0.36$	$3.28^{+0.34}_{-0.33}$	$3.14^{+0.31}_{-0.31}$	$3.17^{+0.23}_{-0.23}$	$3.25^{+0.23}_{-0.23}$	738	Q5-Q12
3	KIC 3424541	$2.43^{+0.08}_{-0.08}$	$84.90^{+4.10}_{-5.50}$	$26.88^{+0.84}_{-0.86}$	$29.80 \pm 2.98$	$3.46 \pm 0.33$	$2.69^{+0.27}_{-0.32}$	$3.34^{+0.32}_{-0.23}$	$2.27^{+0.23}_{-0.23}$	$1.80^{+0.27}_{-0.24}$	1148	Q5-Q17
4	KIC 6116048	$0.71^{+0.08}_{-0.06}$	$65.30^{+12.10}_{-9.50}$	$3.57^{+0.15}_{-0.14}$	$4.00 \pm 0.40$	$17.26 \pm 1.96$	$0.79^{+0.11}_{-0.09}$	$0.67^{+0.08}_{-0.08}$	$0.59^{+0.13}_{-0.15}$	$0.78^{+0.24}_{-0.20}$	738	Q5-Q12
5	KIC 6508366	$2.25^{+0.07}_{-0.07}$	$83.90^{+4.70}_{-6.00}$	$20.87^{+0.59}_{-0.61}$	$18.20 \pm 1.82$	$3.70 \pm 0.35$	$1.96^{+0.20}_{-0.20}$	$3.13^{+0.29}_{-0.29}$	$2.50^{+0.19}_{-0.19}$	$1.58^{+0.26}_{-0.26}$	738	Q5-Q12
6	KIC 6679371	$1.91^{+0.09}_{-0.07}$	$82.00^{+5.50}_{-6.50}$	$17.88^{+0.67}_{-0.64}$	$19.20 \pm 1.92$	$5.48 \pm 0.50$	$2.06^{+0.21}_{-0.21}$	$2.11^{+0.19}_{-0.19}$	$1.85^{+0.17}_{-0.16}$	$1.82^{+0.18}_{-0.16}$	738	Q5-Q12
7	KIC 7103006	$2.43^{+0.23}_{-0.18}$	$44.30^{+4.00}_{-4.50}$	$14.37^{+0.73}_{-0.79}$	$13.20 \pm 1.32$	$4.62 \pm 0.48$	$2.23^{+0.29}_{-0.27}$	$2.50^{+0.26}_{-0.26}$	$2.62^{+0.36}_{-0.34}$	$2.39^{+0.48}_{-0.42}$	738	Q5-Q12
8	KIC 7206837	$2.06^{+0.53}_{-0.50}$	$38.90^{+10.60}_{-6.60}$	$8.80^{+1.12}_{-1.10}$	$10.10 \pm 1.02$	$4.04 \pm 0.28$	$2.34^{+0.45}_{-0.48}$	$2.86^{+0.20}_{-0.20}$	$1.80^{+0.78}_{-0.66}$	$1.51^{+1.10}_{-0.89}$	738	Q5-Q12
9	KIC 9139151	$1.03^{+0.21}_{-0.11}$	$65.00^{+15.00}_{-13.60}$	$4.79^{+0.29}_{-0.28}$	$6.00 \pm 0.60$	$10.96 \pm 2.22$	$1.31^{+0.22}_{-0.17}$	$1.05^{+0.21}_{-0.21}$	$0.73^{+0.28}_{-0.23}$	$1.06^{+0.50}_{-0.40}$	738	Q5-Q12
10	KIC 9139163	$3.20^{+0.39}_{-0.34}$	$28.00^{+3.50}_{-4.00}$	$10.15^{+0.94}_{-0.97}$	$4.00 \pm 0.40$	$6.10 \pm 0.47$	$1.26^{+0.21}_{-0.18}$	$1.89^{+0.19}_{-0.19}$	$4.83^{+0.65}_{-0.56}$	$4.32^{+0.74}_{-0.63}$	738	Q5-Q12
11	KIC 9206432	$1.71^{+1.27}_{-0.43}$	$42.50^{+12.2}_{-18.1}$	$7.77^{+0.99}_{-0.98}$	$6.70 \pm 0.67$	$8.80 \pm 1.06$	$1.51^{+0.87}_{-0.34}$	$1.31^{+0.16}_{-0.16}$	$1.92^{+1.50}_{-0.57}$	$2.02^{+2.20}_{-0.72}$	738	Q5-Q12
12	KIC 9812850	$1.72^{+0.26}_{-0.14}$	$74.70^{+11.70}_{-15.20}$	$12.98^{+0.81}_{-0.74}$	$12.90 \pm 1.29$	$5.19 \pm 0.79$	$1.73^{+0.24}_{-0.19}$	$2.22^{+0.34}_{-0.34}$	$1.77^{+0.38}_{-0.30}$	$1.26^{+0.60}_{-0.48}$	738	Q5-Q12
13	KIC 10162436	$2.24^{+0.15}_{-0.15}$	$24.20^{+2.10}_{-2.50}$	$7.81^{+0.55}_{-0.77}$	$6.50 \pm 0.65$	$11.96 \pm 2.05$	$1.84^{+0.25}_{-0.26}$	$0.96^{+0.17}_{-0.17}$	$2.85^{+0.46}_{-0.57}$	$4.29^{+0.50}_{-0.55}$	738	Q5-Q12
14	KIC 10355856	$1.38^{+0.22}_{-0.15}$	$71.40^{+13.10}_{-13.50}$	$9.74^{+0.82}_{-0.80}$	$7.20 \pm 0.72$	$4.47 \pm 0.31$	$1.03^{+0.16}_{-0.12}$	$2.59^{+0.18}_{-0.18}$	$1.69^{+0.33}_{-0.26}$	$0.49^{+0.48}_{-0.29}$	462	Q5-Q9
15	KIC 10454113	$1.11^{+0.51}_{-0.32}$	$43.50^{+26.00}_{-13.50}$	$4.33^{+0.46}_{-0.46}$	$5.50 \pm 0.55$	$14.61 \pm 1.09$	$1.41^{+0.56}_{-0.37}$	$0.79^{+0.06}_{-0.06}$	$0.79^{+0.55}_{-0.34}$	$1.48^{+1.07}_{-0.68}$	738	Q5-Q12
16	KIC 11253226	$2.88^{+0.29}_{-0.22}$	$75.00^{+10.50}_{-12.00}$	$19.28^{+1.22}_{-1.26}$	$15.1 \pm 1.51$	$3.64 \pm 0.37$	$2.26^{+0.28}_{-0.25}$	$3.17^{+0.32}_{-0.32}$	$3.32^{+0.43}_{-0.38}$	$2.72^{+0.53}_{-0.44}$	276	Q5-Q7
17	KIC 12009504	$1.28^{+0.06}_{-0.07}$	$72.10^{+7.20}_{-5.60}$	$7.32^{+0.23}_{-0.23}$	$8.40 \pm 0.84$	$9.39 \pm 0.68$	$1.46^{+0.15}_{-0.15}$	$1.23^{+0.09}_{-0.09}$	$1.12^{+0.16}_{-0.16}$	$1.33^{+0.15}_{-0.15}$	738	Q5-Q12
18	KIC 12258514	$0.56^{+0.35}_{-0.22}$	$34.50^{+30.30}_{-12.10}$	$2.16^{+0.27}_{-0.26}$	$3.50 \pm 0.35$	$15.00 \pm 1.84$	$0.91^{+0.46}_{-0.33}$	$0.77^{+0.09}_{-0.09}$	$0.63^{+0.88}_{-0.51}$	$1.11^{+1.22}_{-0.78}$	738	Q5-Q12
19	<i>Kepler-25</i>	$1.73^{+0.14}_{-0.20}$	$67.10^{+11.20}_{-7.60}$	$9.18^{+0.61}_{-0.70}$	$9.50 \pm 0.50$	/	$1.76^{+0.15}_{-0.13}$	/	$1.69^{+0.27}_{-0.33}$	/	1114	Q5-Q16
20	HAT-P-7	$0.68^{+1.04}_{-0.41}$	$27.80^{+35.40}_{-18.20}$	$2.95^{+1.68}_{-1.97}$	$3.80 \pm 0.50$	/	$0.92^{+1.53}_{-0.42}$	/	$1.02^{+2.90}_{-0.71}$	/	1437	Q0-Q16
21	HD 49933	$2.42^{+1.70}_{-1.09}$	$25.70^{+16.20}_{-7.20}$	$7.31^{+2.45}_{-2.21}$	$10.00 \pm 0.50$	$3.40 \pm 0.40^{(a)}$	$3.58^{+1.28}_{-1.23}$	$3.40^{+0.40}_{-0.40}$	$2.00^{+2.55}_{-1.16}$	$2.54^{+3.02}_{-1.82}$	180	/
22	HD 181420	$2.86^{+0.62}_{-0.53}$	$53.70^{+14.60}_{-10.10}$	$16.31^{+2.12}_{-2.32}$	$18.00 \pm 1.00$	$2.56 \pm 0.57^{(a)}$	$3.15^{+0.57}_{-0.43}$	$4.50^{+0.85}_{-0.85}$	$2.69^{+0.81}_{-0.77}$	$1.87^{+1.29}_{-1.05}$	156	/

 (a) Using spot modelling, Mosser et al. (2009) provide alternative surface rotation rate for the CoRoT stars. For HD 49933, they found  $3.45 \pm 0.05$  days and  $2.25 \pm 0.03$  days for HD 181420.

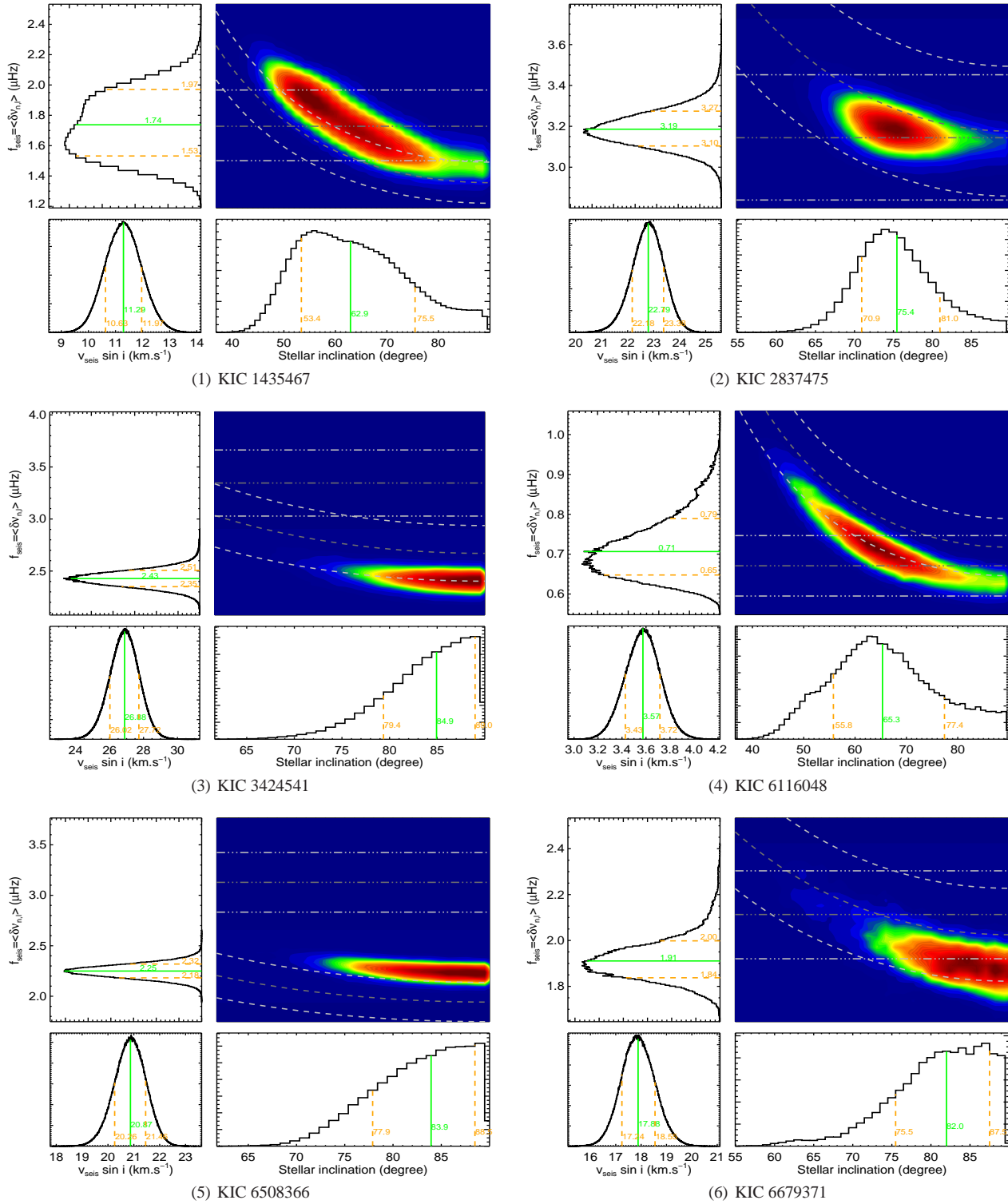


**Figure A1.** Joint-probability density functions for all of the analysed stars. Horizontal dash-dotted lines indicate the surface rotation rates from lightcurve modulation due to spots (when available), while dashed curves are the rotation rates derived using the spectroscopic  $v \sin i$ . Unless specified, all spectrum fit include modes of degree  $l = 0, 1, 2$ .

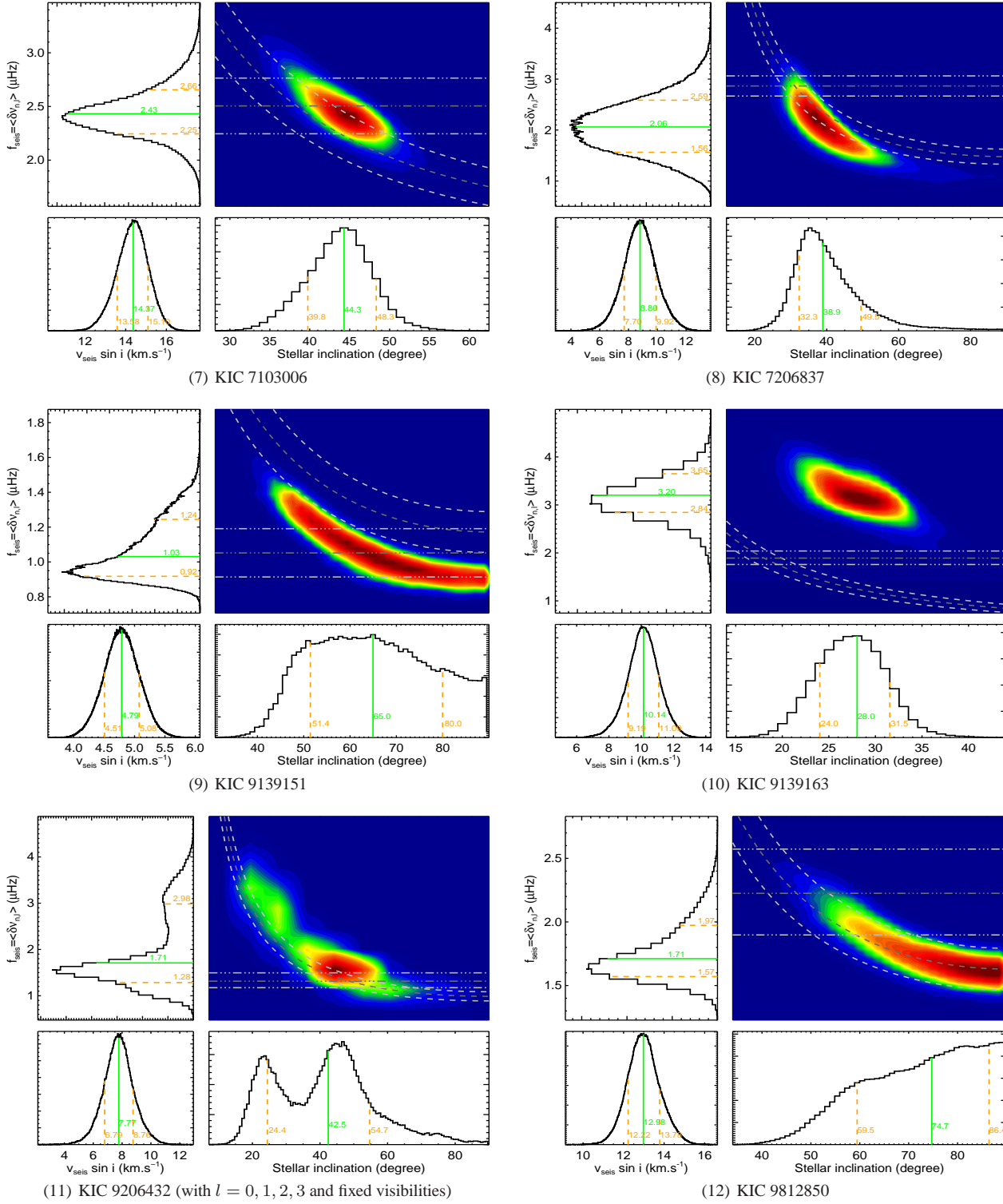


Figure A1 – continued

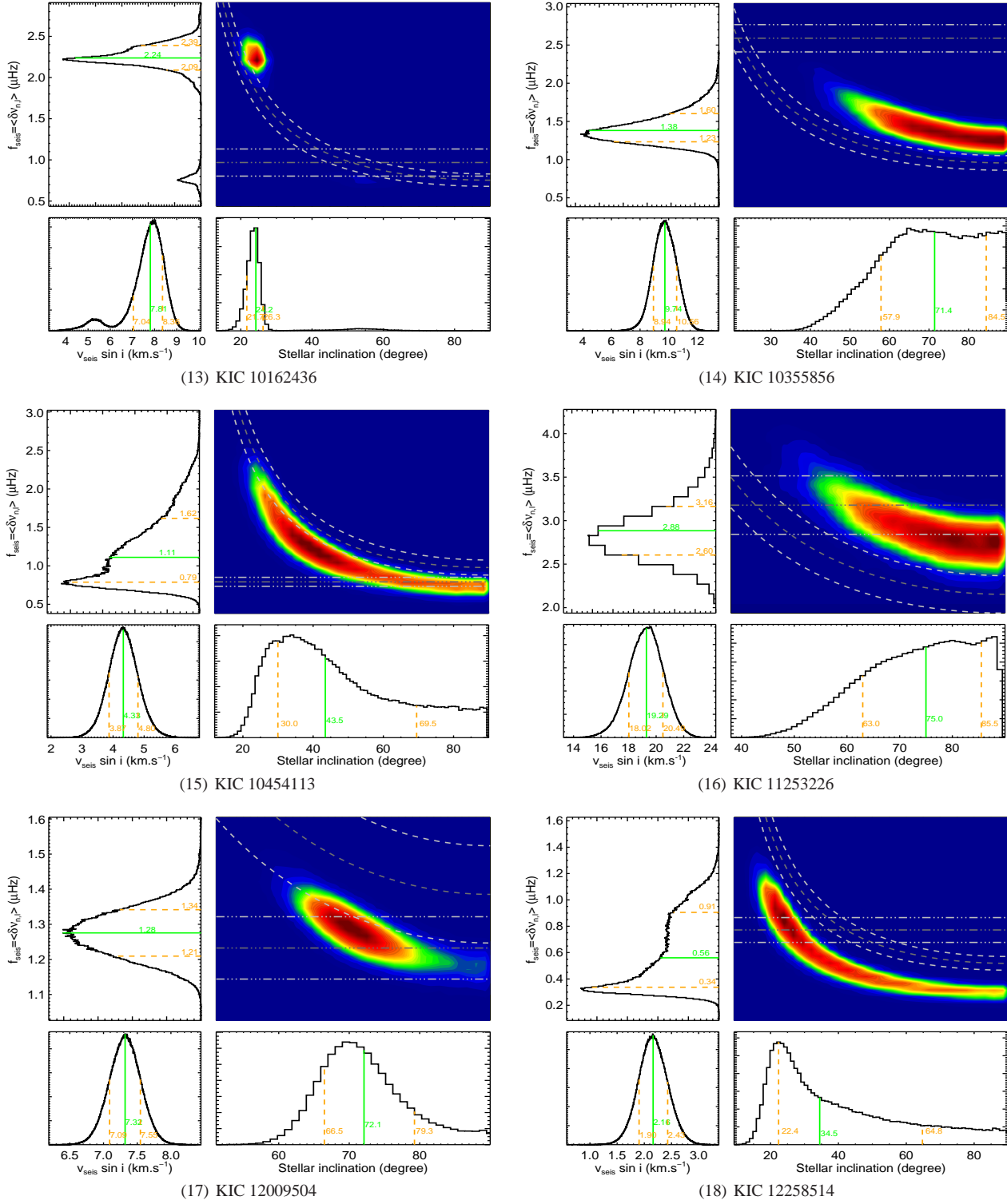


Figure A1 – continued

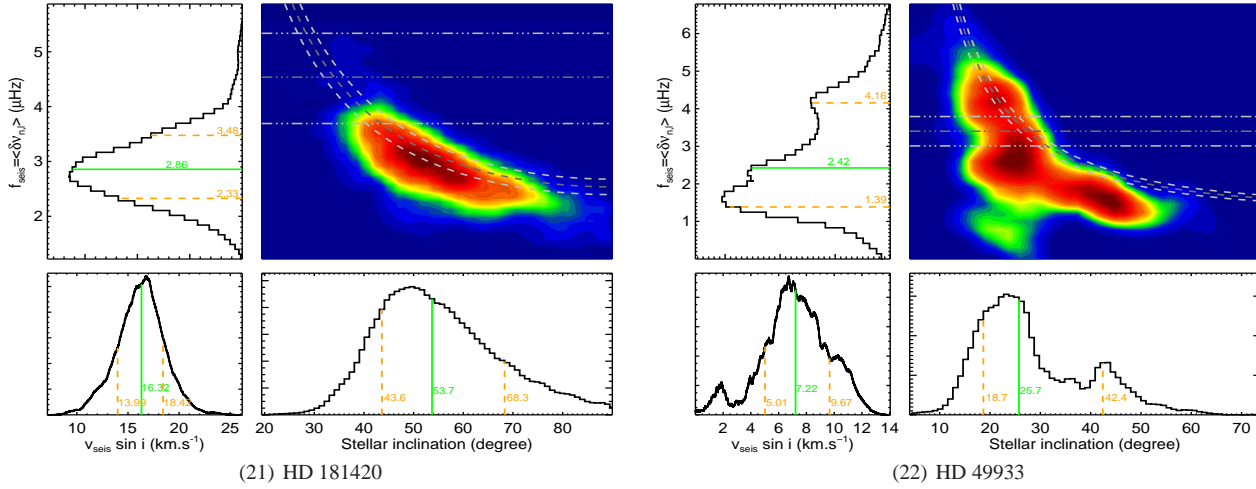
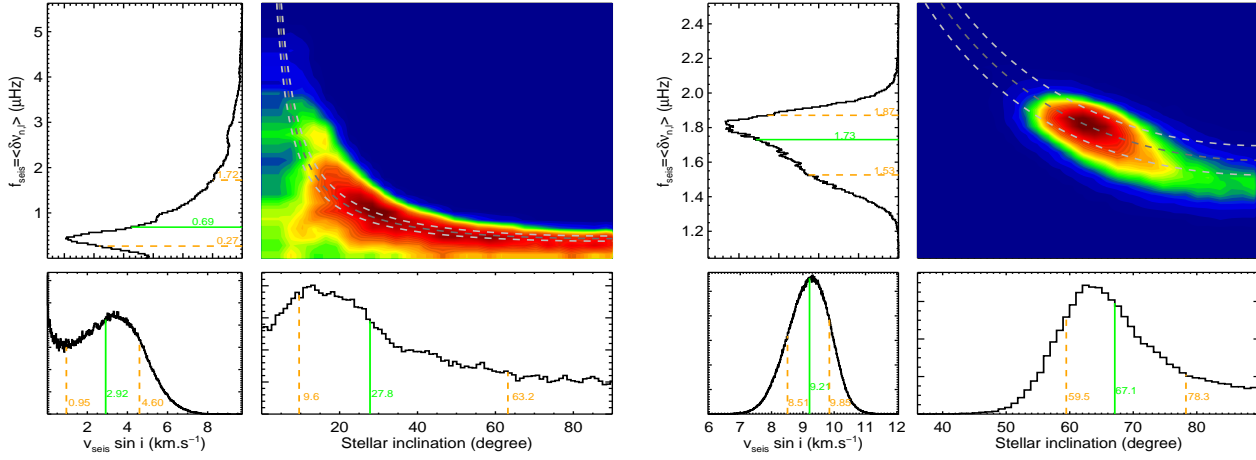


Figure A1 – continued

**APPENDIX B: SUPPLEMENTARY CONTENTS FOR KIC 3424541**

The best fit of the power spectrum for the two possible mode identification of KIC 3424541 is shown in Fig. B1 and Fig. B2. The most probable mode identification was assessed by using the Bayes ratio  $O(M_1, M_2)$  between the two possible competing models  $M_1$  and  $M_2$  (e.g. Benomar, Appourchaux & Baudin 2009).  $O(M_1, M_2)$  is the equivalent of the the likelihood ratio used in frequentist approaches. However, contrary to the likelihood ratio, the Bayes ratio can be interpreted in terms of probability. For example a Bayes ratio of  $O(M_1, M_2)=3$  in favour of  $M_1$  indicates that the model  $M_1$  has 75% of probability to be correct. It is often considered that a model is strongly supported when the ratio exceeds 100 (Jeffreys 1961). In the case of KIC 3424541, the mode identification shown in Fig.B1 is very strongly supported because the logarithm of the Bayes factor is  $7.5 \times 10^3$  in favour of this identification.

The list of measured pulsation frequencies for the most likely mode identification of KIC 3424541 is given in Table B1.

**APPENDIX C: SUPPLEMENTARY CONTENTS FOR KIC 9206432**

Our thorough analysis of KIC 9206432 enabled us to identify the likely cause for the apparent discrepancy between the surface and the interior rotation. In Fig.C1 (top), we show the results for the stellar inclination and the rotational splitting when the power spectrum is fitted by considering the modes visibilities  $V_{l=1}^2$  and  $V_{l=2}^2$  as free parameters. In that case, there is an apparent mismatch between surface rotation and rotational splitting. When the visibilities are fixed to their expected values, the agreement becomes better (middle and bottom).

**Table B1.** Mode frequencies for the most likely mode identification of KIC 3424541 presented in this paper.

degree $l$	index	frequency ( $\mu\text{Hz}$ )
0	1	496.77 $\pm$ 0.58
0	2	535.47 $\pm$ 0.58
0	3	575.46 $\pm$ 0.34
0	4	615.77 $\pm$ 0.35
0	5	658.44 $\pm$ 0.27
0	6	699.47 $\pm$ 0.28
0	7	740.87 $\pm$ 0.32
0	8	781.62 $\pm$ 0.30
0	9	822.33 $\pm$ 0.33
0	10	864.54 $\pm$ 0.41
0	11	905.98 $\pm$ 0.52
0	12	947.90 $\pm$ 0.57
0	13	991.82 $\pm$ 0.67
0	14	1035.99 $\pm$ 1.97
1	1	474.25 $\pm$ 0.61
1	2	514.14 $\pm$ 0.38
1	3	553.20 $\pm$ 0.30
1	4	593.10 $\pm$ 0.25
1	5	634.54 $\pm$ 0.23
1	6	676.47 $\pm$ 0.22
1	7	718.29 $\pm$ 0.23
1	8	759.57 $\pm$ 0.24
1	9	799.76 $\pm$ 0.30
1	10	841.50 $\pm$ 0.36
1	11	883.52 $\pm$ 0.41
1	12	925.42 $\pm$ 0.56
1	13	967.46 $\pm$ 0.55
1	14	1009.04 $\pm$ 1.16
2	1	493.35 $\pm$ 1.67
2	2	533.17 $\pm$ 0.90
2	3	573.26 $\pm$ 0.64
2	4	614.03 $\pm$ 0.53
2	5	655.45 $\pm$ 0.52
2	6	697.51 $\pm$ 0.44
2	7	738.99 $\pm$ 0.51
2	8	781.14 $\pm$ 0.50
2	9	822.45 $\pm$ 0.55
2	10	864.26 $\pm$ 0.63
2	11	905.82 $\pm$ 0.76
2	12	946.56 $\pm$ 1.09
2	13	987.69 $\pm$ 1.46
2	14	1028.68 $\pm$ 2.59

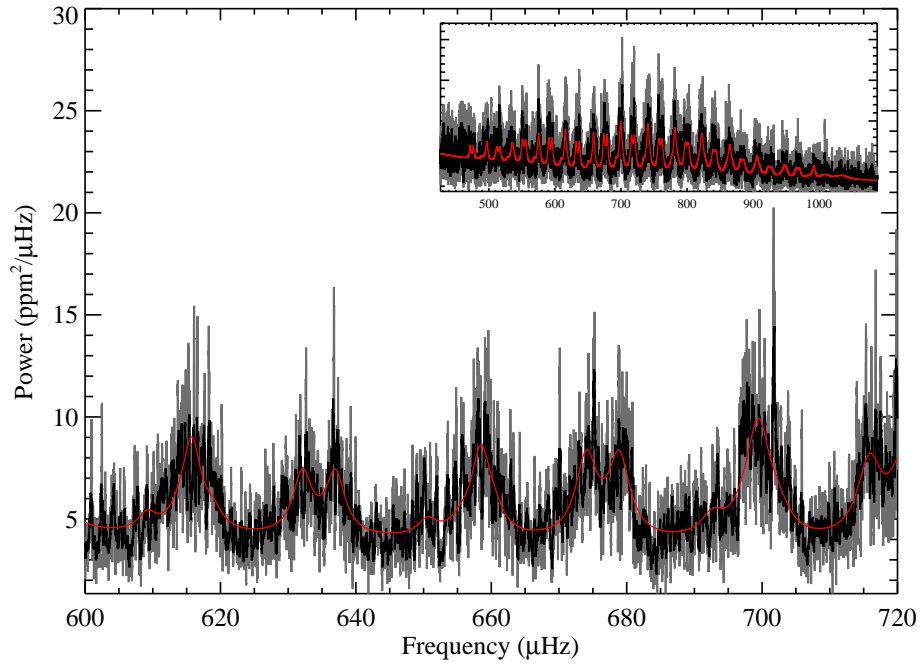


**Figure B1.** Fit of the power spectrum of KIC 3424541 with the most likely mode identification (opposite as in Appourchaux et al. (2012)), obtained from the *Kepler* data analysis using Quarters 5 to 17. In this identification, the first excess of power on the left of the figure is due to a pair of degree  $l = 2, 0$ , and is followed by alternating  $l = 1$  and  $l = 2, 0$  modes.

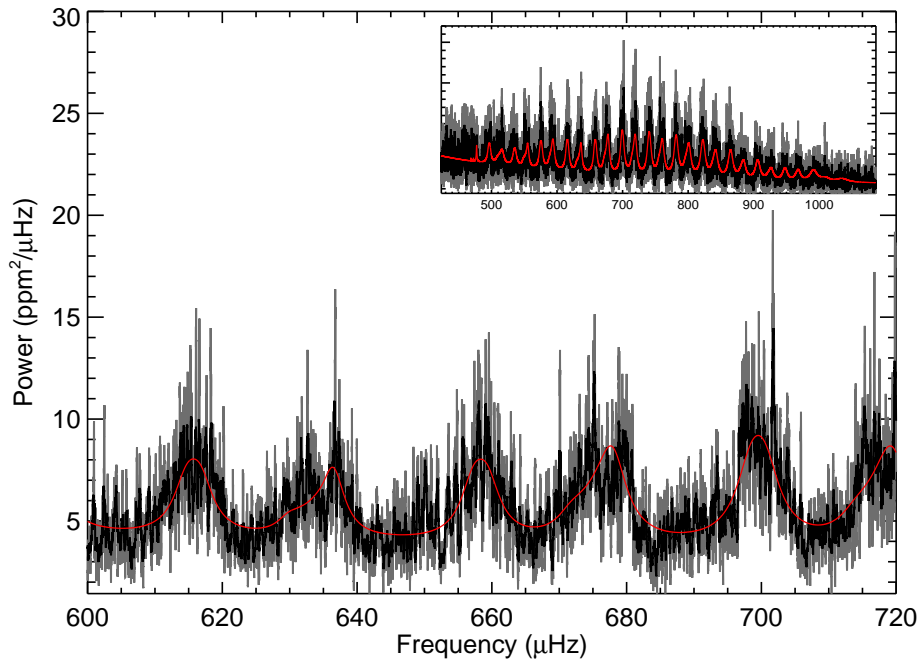


**Figure B2.** Fit of the power spectrum of KIC 3424541 with the less likely mode identification (same as in Appourchaux et al. (2012)), obtained from the *Kepler* data analysis using Quarters 5 to 17. In this identification, the first excess of power on the left of the figure corresponds to a degree  $l = 1$ , and is followed by alternating  $l = 2, 0$  and  $l = 1$  modes.

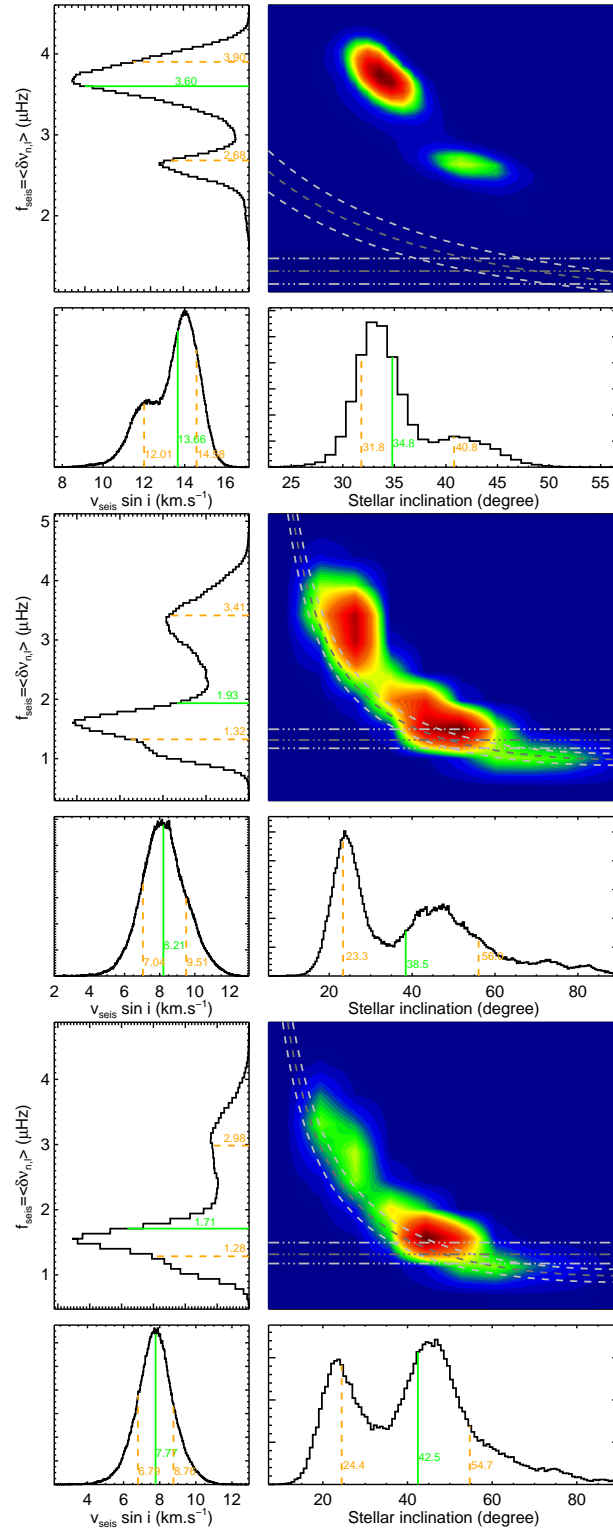


**Figure C1. KIC 9206432.** Comparison of the results obtained for the stellar inclination and rotational splitting by including; (top) modes of degree  $l = 0, 1, 2$  mode visibilities as free parameters; (middle) modes of degree  $l = 0, 1, 2$  with fixed visibilities; (bottom) modes of degree  $l = 0, 1, 2, 3$  with fixed visibilities.